



HAL
open science

Pseudoprogession versus true progression in glioblastoma patients: A multiapproach literature review. Part 2-Radiological features and metric markers

Caroline Bund, Benjamin Leroy-Freschini, Roland Schott, Helene Cebula, Georges Noel, Clara Le Fevre, Jean-Marc Constans, Isabelle Chambrelant, Delphine Antoni

► To cite this version:

Caroline Bund, Benjamin Leroy-Freschini, Roland Schott, Helene Cebula, Georges Noel, et al.. Pseudoprogession versus true progression in glioblastoma patients: A multiapproach literature review. Part 2-Radiological features and metric markers. *Critical Reviews in Oncology/Hematology*, 2021, 159, 10.1016/j.critrevonc.2021.103230 . hal-03599517

HAL Id: hal-03599517

<https://u-picardie.hal.science/hal-03599517v1>

Submitted on 13 Feb 2023

HAL is a multi-disciplinary open access archive for the deposit and dissemination of scientific research documents, whether they are published or not. The documents may come from teaching and research institutions in France or abroad, or from public or private research centers.

L'archive ouverte pluridisciplinaire **HAL**, est destinée au dépôt et à la diffusion de documents scientifiques de niveau recherche, publiés ou non, émanant des établissements d'enseignement et de recherche français ou étrangers, des laboratoires publics ou privés.



Distributed under a Creative Commons Attribution - NonCommercial 4.0 International License

Pseudoprogession versus true progression in glioblastoma patients: a multiapproach literature review. Part 2 – Radiological features and metric markers.

Clara Le Fèvre¹, MD MSc, Jean-Marc Constans², MD PhD, Isabelle Chambrelant¹, MSc, Delphine Antoni¹, MD MSc, Caroline Bund³, MD MSc, Benjamin Leroy-Freschini³, MD, Roland Schott⁴, MD MSc, Hélène Cebula⁵, MD MSc, Georges Noël^{1*}, MD PhD.

¹ Department of radiotherapy, ICANS, Institut Cancérologie Strasbourg Europe, 17 rue Albert Calmette, 67200 Strasbourg Cedex, France.

² Department of Radiology, Amiens-Picardie University Hospital, 1 rond-point du Professeur Christian Cabrol, 80054 Amiens Cedex 1, France.

³ Department of Nuclear Medicine, ICANS, Institut Cancérologie Strasbourg Europe, 17 rue Albert Calmette, 67200 Strasbourg Cedex, France.

⁴ Departement of medical oncology, ICANS, Institut Cancérologie Strasbourg Europe, 17 rue Albert Calmette, 67200 Strasbourg Cedex, France.

⁵ Departement of Neurosurgery, Hautepierre University Hospital, 1, avenue Molière, 67200 Strasbourg, France

*: Corresponding author: Pr Georges NOEL, Department of radiotherapy, ICANS, Institut Cancérologie
Strasbourg Europe, 17 rue Albert Calmette, 67200 Strasbourg Cedex, France, +33 368766969,
g.noel@icans.eu

Clara Le Fèvre¹, MD MSc: c.lefevre@icans.eu

Jean-Marc Constans², MD PhD: constans.jean-marc@chu-amiens.fr

Isabelle Chambrelant¹MSc: i.chambrelant@icans.eu

Delphine Antoni¹, MD MSc: d.antoni@icans.eu

Caroline Bund³, MD MSc: c.bund@icans.eu

Benjamin Leroy-Freschini³, MD: b.leroy-freschini@icans.eu

Roland Schott⁴, MD MSc: r.schott@icans.eu

Hélène Cebula⁵, MD MSc: helene.cebula@chru-strasbourg.fr

Georges Noël^{1*}, MD PhD: g.noel@icans.eu

Pseudoprogession versus true progression in glioblastoma patients: a multiapproach literature review.

Part 2 – Radiological features and metric markers.

Highlights

- Patients treated for glioblastoma can experience pseudoprogression
- Differentiating pseudoprogression and true progression is challenging
- A review of predictive imaging markers of pseudoprogression was performed
- Conventional MRI, advanced MRI, spectroscopy and PET features were analyzed

Abstract

After chemoradiotherapy for glioblastoma, pseudoprogression can occur and must be distinguished from true progression to correctly manage glioblastoma treatment and follow-up. Conventional treatment response assessment is evaluated via conventional MRI (contrast-enhanced T1-weighted and T2/FLAIR), which is unreliable. The emergence of advanced MRI techniques, MR spectroscopy, and PET tracers has improved pseudoprogression diagnostic accuracy. This review presents a literature review of the different imaging techniques and potential imaging biomarkers to differentiate pseudoprogression from true progression.

Key words

Diffusion MRI, Glioblastoma, MRS, Perfusion MRI, PET tracers, Pseudoprogression, Progression

1 **1. Introduction**

2 The estimated number of new brain and nervous system cancer cases in the United States in
3 2020 was 23 890, and there were 18 020 estimated deaths in the same year [1]. Glioblastoma
4 multiforme (GBM), the most common malignant brain primary tumor in adults, represents
5 approximately 60% of all gliomas [2–4]. The incidence of GBM is 3/100,000 in Europe and
6 North America (12 000 patients per year) [5–7]. One-third of patients with GBM survive 1
7 year, with a median survival of 15 to 18 months, and the survival rate is less than 5% at 5
8 years [2,3,8–11], even with improvements in chemoradiotherapy (CRT) [8,12,13]. In a
9 systematic review, the authors established that the 10-year survival rate was 0.71% [14].
10 Since the introduction of CRT and adjuvant temozolomide (TMZ) following surgery, more
11 patients with GBM have experienced pseudoprogression (PsP) [15–17] than those receiving
12 radiotherapy (RT) alone [8]. PsP is usually a subacute effect that occurs in the first six months
13 after CRT [18–28]. It mimics progression that evokes response to treatment rather than
14 treatment failure [19,25,29,30]. Its incidence remains variable; the literature reports rates from
15 2% to more than 50%, with a rate of 36% in a recent meta-analysis [31]. During magnetic
16 resonance imaging (MRI) follow-up of patients treated with surgery, CRT and adjuvant TMZ
17 for GBM, suspected images of progression can occur at the site of previously treated GBM or
18 at distant sites. Progression is suspected when conventional MRI shows new or enlarged
19 contrast-enhancing imaging compared to presurgery, postsurgery, or pre-RT MRI [18]. To
20 differentiate between PsP and true progression (TP), MRI is often repeated 4 to 8 weeks after
21 the MRI showing progression in the absence of pathological proof [32]. However, the images
22 *per se* are not specific to PsP or TP.

23 Some groups have proposed criteria to guide response assessment to treatment, but those
24 criteria have limits [33–37]. The Macdonald criteria were the first to measure radiological
25 response through the two-dimensional measurement of contrast enhancement [35]. In 2010,

1 the RANO criteria took into account T2/FLAIR signal changes in addition to contrast 2D
2 enhancement measurements [34]. Modified criteria were published for immune therapies and
3 other clinical situations [33,37]. No single imaging feature or combination of features have
4 been validated to date to differentiate PsP and TP [38]. New therapeutics that impact MRI
5 further complicate PsP diagnosis. Moreover, contrast-enhanced image signal MRI is
6 dependent on the contrast dose, injection timing, magnetic field strength, and choice of image
7 sequences [32]. Conventional MRI is limited in response assessment and disease progression
8 monitoring. Some authors proposed evaluation of advanced imaging, now routinely available,
9 to find noninvasive imaging markers, improve PsP diagnosis, and improve patient outcome
10 [39,40]. In addition to supplying structural and anatomical information, advanced MRI
11 provides cellular, biological, and metabolic information [41]. A meta-analysis including 941
12 patients with GBM showed that advanced MRI techniques had higher diagnostic accuracy
13 than conventional MRI for the distinction of PsP and TP, with a sensitivity and specificity of
14 71-92% and 85-95% vs 68% and 77%, respectively. Magnetic resonance spectroscopy (MRS)
15 had the best accuracy with a sensitivity and specificity of 91% and 95%, respectively,
16 followed by perfusion MRI with dynamic contrast-enhanced MRI (DCE) [42]. The authors
17 developed a model-based metric of therapy response based on T1 contrast-enhanced MRI and
18 used linear, 4D-spherical, and 4D-anatomic models to distinguish PsP from TP with a
19 sensitivity of 79%, a specificity of 59%, a positive predictive value (PPV) of 50%, and a
20 negative predictive value (NPV) of 93% [43]. The combination of advanced modalities in
21 multiparametric imaging improves accuracy but requires training, clinical trial data, and
22 standardization.

23 The aim of this analytic review was to discuss the metrics of diffusion MRI, perfusion MRI,
24 MRS, and positron emission tomography (PET) techniques to distinguish PsP from TP.

25 **2. Methods**

1 A literature search was conducted using the Medline/PubMed, ScienceDirect, and Cochrane
2 Wiley databases. The search terms used included (“glioblastoma” OR “gliomas” OR “high
3 grade gliomas”) AND (“pseudoprogession” OR “pseudo-progression”). Articles concerning
4 PsP in adult patients treated for glioma, high-grade glioma (HGG) and glioblastoma treated
5 with the Stupp protocol were examined. References provided from relevant articles were also
6 examined to identify additional studies for inclusion. Any irrelevant entries and non-English
7 articles were excluded. A total of 23 articles about conventional MRI, 43 about diffusion
8 MRI, 58 about perfusion MRI, 25 about MRS, 59 about PET scan, and 14 about SPECT were
9 included in this review.

10 **3. Conventional MRI**

11 Conventional gadolinium contrast-enhanced MRI is the gold standard for the measurement of
12 response to treatment but is not efficient in distinguishing TP from PsP [29]. Conventionally,
13 PsP MR images show vasogenic edema due to increased vascular permeability and increased
14 contrast enhancement [19,44]. Santra *et al.* included 90 patients (16 of whom had GBM) and
15 concluded that the overall sensitivity, specificity, PPV, NPV and accuracy of conventional
16 MRI to detect TP were 83%, 25%, 77%, 33%, and 67%, respectively [45]. For the follow-up
17 of GBM patients treated with CRT, the National Comprehensive Cancer Network (NCCN)
18 suggests 1) preoperative MRI, 2) intraoperative MRI for optimal tumor resection (when
19 available), 3) 48-72 h postoperative MRI, 4) 4-week post-CRT MRI, and 5) repeat MRI every
20 2–4 months according to the disease status and clinical course [46]. To assist clinicians in PsP
21 diagnosis and uniform practices, the International Standardized Brain Tumor Imaging
22 Protocol (BTIP) established the minimum image acquisition requirements for 1.5T and 3T
23 MR scans: sagittal/axial T1, axial FLAIR and axial DWI prior to contrast administration, and
24 axial T2 and sagittal/axial T1 after contrast administration [36].

25 **3.1.T1-weighted contrast-enhanced images**

1 Some studies reported that the size of enhancing lesions was higher in TP than in PsP [47,48].
2 Several TP radiological markers were identified to indicate the involvement of the corpus
3 callosum, including either multiple enhancing foci crossing the midline and multiple
4 enhancing lesions or subependymal spread and multiple enhancing lesions [49],
5 subependymal enhancement [50,51], spreading wave front of enhancement [51], the
6 enhancing lesion crossing the midline [47], and solid enhancement with distinct margins and
7 focally enhancing nodules [52]. Hansen *et al.*, in a study including 15 GBM patients with
8 40% unmethylated MGMT promoters and 67% IDH1 wild-type, showed that in 3D MRI, a
9 more spherical, more symmetric and fuller contrast enhancement with reduced perforations in
10 the outer shell of the enhanced region was conducted for TP diagnosis [53]. However, some
11 studies showed that the increase in T1 contrast enhancement was not statistically significant
12 between PsP and TP [20], and the change in the size of the enhancing lesion between baseline
13 MRI and MRI at progression was not a determinant criterion between PsP and TP [47]. In the
14 Agarwal *et al.* study including 46 HGGs, no difference was found in the location of the
15 recurrent volume between PsP and TP [47]. Moreover, no correlation between MRI changes
16 and radiation dose distribution was demonstrated between PsP and TP [47]. The authors
17 showed that the sharp demarcation was poorly defined in PsP compared to TP [47]. Young *et*
18 *al.* analyzed 93 GBM patients and demonstrated that new enhancement, marginal
19 enhancement, nodular enhancement, callosal enhancement, a spreading wave front of
20 enhancement, cystic or necrotic changes, increased peritumoral intensity, subsequent
21 decreased enhancement, and diffusion restrictions were not predictive factors of PsP [50].
22 Textural feature analysis of conventional MRI could help differentiate PsP and TP [54].
23 The interpretation of T1-weighted enhanced MR images can be prudent because they may be
24 influenced by radiological techniques, corticosteroid use [55], antiangiogenic agents [56] or
25 MGMT promoter methylation [15]. Moreover, differential nontumoral diagnoses of

1 enhancing lesions can be performed, such as inflammation, seizure, postsurgical changes, and
2 ischemia.

3 **3.2.T2/FLAIR**

4 A trend toward an increase in FLAIR signal intensity in TP [47,57] was discussed [20]. Some
5 authors showed an increase in the FLAIR volume favoring TP [58] as the bidimensional size
6 measurement increased [47]. Moreover, the FLAIR volume in the 45 Gy (75%) isodose
7 favored PsP [58].

8 The T2/FLAIR signal must be interpreted with caution because it can be influenced by
9 treatment effects, corticosteroids, demyelination, infection, or seizure [34].

10 Due to the similarities between PsP and TP on conventional MRI and the difficulties faced by
11 clinicians and neuroradiologists, advanced imaging techniques, such as MRS, diffusion-
12 weighted MRI (DWI), MR perfusion imaging, diffusion-tensor imaging and PET-based
13 strategies, are necessary [59,60]. Multiple sequences were developed to allow several metric
14 measurements, and they are described in Table 1.

15 **4. Diffusion-weighted MRI (DWI) and Diffusion tensor imaging (DTI)**

16 Advanced MRI techniques can provide additional information when conventional MRI is
17 ambiguous to improve the distinction between PsP and TP [39,61]. Different diffusion
18 modalities and metrics were developed (Table 1) [30,62,63]. Radiation injury images usually
19 show heterogeneity on DWI images and often include spotty and marked hypointensity [64].
20 Analyzing signal intensity patterns on DWI, Lee *et al.* showed, in a study enrolling 22 HGG
21 patients (10 with TP, including six that were MGMT promotor methylated, and 12 with PsP,
22 including five that were MGMT promotor methylated), that patients with TP had a higher
23 incidence of homogeneous or multifocal high signal intensity than those with PsP who had
24 rim high or no high intensity signal ($p=0.027$). The PsP volume was higher than the TP
25 volume ($p=0.009$) [65]. Xu *et al.* concluded, in a study of 35 patients, that DTI offered a

1 sensitivity, specificity, PPV, and NPV of 85%, 87%, 89%, and 81%, respectively. The lesion
2 classification accuracy was 86% [66].

3 **4.1. Apparent Diffusion Coefficient (ADC)**

4 ADC helps to distinguish whether enhancing lesions result from TP with the hypothesis that
5 recurrent tumors have low ADC values [30,44,64,67–72]. Van Dijken *et al.*, in a meta-
6 analysis of 35 studies and 1174 patients, retrieved an ADC pooled sensitivity and specificity
7 of 71% and 87%, respectively, to differentiate PsP and TP [42]. Some authors reported that
8 ADC values and ADC ratios were higher in PsP patients than in TP patients [64,66,67,73–80],
9 but others did not demonstrate a difference [47,68,81] (Table 2). Al Sayyari *et al.* used
10 susceptibility-weighted imaging (SWI), which is useful in visualizing heterogeneous tissue
11 patterns; providing information on microvasculature, necrosis, and the blood-brain barrier; and
12 evaluating ADC values in the context of an abnormal blood-brain barrier. The authors
13 compared contrast-enhanced T1-weighted imaging (CE-T1) and contrast-enhanced
14 susceptibility-weighted imaging (CE-SWI) of 17 patients with new contrast enhancement
15 after CRT and created ADC maps. They reported that the CE-SWI volume was reduced
16 compared to CE-T1 volume ($p=0.002$), with no difference in the median ADC value. An
17 increase in CE-SWI volume was associated with a trend toward reduced ADC in TP. Patients
18 with TP had significantly reduced ADC values vs patients with PsP who had significantly
19 elevated ADC values within the CE-SWI enhancement volume [82]. The fifth percentile of
20 ADC maps could be helpful for distinguishing PsP and TP. Song *et al.* proposed a threshold
21 value of the fifth percentile of $0.892 \times 10^{-3} \text{ mm}^2/\text{s}$ to differentiate PsP and TP with a
22 sensitivity of 90% and a specificity of 90% in a study including 20 GBM patients with 70%
23 methylated MGMT promoters (10 each in the TP and PsP groups) [83]. Chu *et al.* analyzed
24 histograms of ADC maps in 30 GBM patients, of whom 15 were methylated in both the TP
25 and PsP groups and 40% were methylated in the MGMT promoter. The fifth percentile was

1 significantly lower in TP than in PsP regardless of standard or high b value ($p=0.049$ and
2 $p<0.001$, respectively). The authors concluded that the fifth percentile of the cumulative ADC
3 histogram was a promising parameter with an accuracy of 89% for high b values (b3000) and
4 67% for standard b values (b1000) [84].

5 **4.2.Fractional Anisotropy (FA)**

6 The FA value was higher in TP than in PsP in some studies [66,78,85], but some authors
7 reported no difference [47,68]. Alexiou *et al.* proposed an FA ratio cutoff value of >0.47 for
8 TP with 57% sensitivity and 100% specificity in a study that included 30 HGG patients [78].
9 In Xu *et al.*'s study, TP was suggested when either an ADC ratio <1.65 or/and an FA ratio
10 >0.36 was detected in the contrast-enhancing lesion [66]. Wang *et al.* showed that an FA
11 threshold value of >0.13 to diagnose TP had a sensitivity of 71% and a specificity of 75% in
12 41 GBM patients [85].

13 The sensitivity of diffusion MRI was probably sufficient to differentiate PsP and TP, but the
14 specificity remained low [44]. Larger studies with more sophisticated and especially precise
15 analytical techniques are required to determine uniform diffusion parameters.

16 **5. Perfusion imaging findings**

17 In a recent European survey, perfusion MRI (table 1) seemed to be used most frequently to
18 differentiate TP and radiation effects [86]. Optimal thresholds must be determined and
19 validated prospectively to confirm that the accuracy is sufficient for clinical use.

20 **5.1.Dynamic susceptibility contrast MRI (DSC)**

21 DSC is the most used perfusion modality. An inherent limitation of DSC is underestimation
22 of the blood volume in areas of significant blood-brain barrier breakdown [87]. TP is usually
23 characterized by increased blood volume and blood flow secondary to neocapillary formation
24 and dilation of preexisting vasculature, leading to an increase in the relative cerebral blood
25 volume (rCBV) compared to PsP, which is always typified by a decrease in rCBV [88,89]. A

1 meta-analysis investigated 28 studies and 1743 patients and reported that DSC had a
2 sensitivity of 89% and a specificity of 80% to diagnose PsP. With a mean rCBV ranging from
3 0.9 to 2.15 and a maximum rCBV ranging from 1.49 to 3.1, the sensitivity and specificity to
4 detect TP were 88%/88% and 93%/76%, respectively [90]. Van Dijken *et al.* reported a DSC
5 pooled sensitivity and specificity of 87% and 86%, respectively, to diagnose TP [42].
6 In some studies, rCBV was significantly higher in TP than in PsP [28,75–78,81,85,91–102],
7 but a few studies demonstrated no difference [20,83,103–105](Table 3). Mangla *et al.*
8 showed, in 36 GBM patients, PsPs and TPs had a mean decrease in rCBV of 41% and 12%,
9 respectively, at one month after CRT [106]. Kong *et al.* prospectively studied DSC in 59
10 GBM patients with new or enlarged enhancing lesions after CRT and 41% MGMT promoter
11 methylation. A significant difference was observed in rCBV between PsP (0.87) and TP
12 (3.25) for patients with an unmethylated O⁶-methylguanine-DNA methyltransferase (MGMT)
13 promoter (p=0.009), while no significant difference was found between rCBV in PsP and
14 rCBV in TP for patients with MGMT promoter methylation (1.56 vs 2.34, p=0.258) [107].
15 Analyzing changes in kurtosis and skewness derived from normalized rCBV between the first
16 and second post-CRT follow-up of 79 patients with GBM as an imaging biomarker predictor
17 for early treatment response to CRT, Baek *et al.* demonstrated that histogram parameters
18 (maximum, mode, range, percent change of skewness and kurtosis, and histographic patterns)
19 showed significant differences between PsP and TP. In multivariate analysis, maximum and
20 histographic patterns were independent predictors of TP. Histogram analysis of rCBV can
21 help to differentiate PsP from TP with a sensitivity of 85.7% and a specificity of 89.2% [108].
22 rPH and PSR were found to be significantly higher and lower, respectively, in TP patients
23 than in PsP patients [91,100]. However, some authors disputed the difference determined by
24 PSR [77].

25 **5.2.Dynamic contrast enhanced MRI (DCE)**

1 DCE was identified as biomarker of PsP [109]. K^{trans} was significantly higher in TP patients
2 [92,110–112], including V_e [111] and V_p [112], but some studies did not show differences in
3 V_e [92,105,110], V_p [111] or K_{ep} [105,110] (Table 3). However, the evaluation time seemed
4 longer since Shin *et al.* demonstrated, in a study including 31 gliomas in 18 GBM patients,
5 that rCBV and rK^{trans} were significantly higher in the TP group than in the PsP group three
6 months after CRT ($p=0.007$ and $p=0.026$, respectively) but not within three months ($p=0.511$
7 and $p=0.399$, respectively) [105].

8 A meta-analysis by Van Dijken *et al.* reported a DCE pooled sensitivity and specificity of
9 92% and 85%, respectively, to diagnose TP [42].

10 **5.3.Arterial spin labeling (ASL)**

11 ASL is a less frequently used noninvasive perfusion MRI technique [70,113,114]. ASL can
12 help the distinction between PsP and TP [115]. ASL was an independent predictor of TP
13 (OR=4.73; $p=0.0017$) with a sensitivity of 79%, a specificity of 64% and improved
14 diagnostic accuracy (from 76% to 89%) when interpreted qualitatively in conjunction with
15 DSC [113]. A meta-analysis retrieved estimates of ASL pooled sensitivity and specificity
16 varying from 52% to 79% and from 64% to 82%, respectively [42]. ASL had a higher
17 sensitivity than DSC (94% vs 71%) for diagnosing TP [116]. The rCBF was significantly
18 higher in patients with TP than in those with PsP in some studies [92,102] but not in others
19 [28,92], according to the authors (Table 3).

20 **5.4.Combination of parameters**

21 Multiparametric imaging was useful in the diagnosis of TP vs PsP [117]. Cha *et al.* examined
22 a multiparametric approach combining DWI and perfusion MRI with rCBV and ADC values
23 in 35 patients with GBM (24 with PsP and 11 with TP). Diagnoses based on the
24 multiparametric approach were more accurate than those based on the uniparametric
25 approach, with 82% sensitivity and 100% specificity, and rCBV was the best predictor of TP

1 (p<0.001) [88]. Kim *et al.* performed measurements using two readers in 169 GBM patients
2 (87 with TP and 82 with PsP). They demonstrated that the addition of conventional MRI and
3 DWI with either DSC (p<0.001 and p=0.002 for each reader, respectively) or DCE (p<0.001
4 for both readers) improved the prediction of TP. With the combination of conventional MRI,
5 DWI and DSC, the sensitivity and specificity varied from 82% to 84% and from 95% to 96%,
6 respectively. With the combination of conventional MRI, DWI, and DCE, the sensitivity and
7 specificity varied from 91% to 92% and from 84% to 87%, respectively [51]. Combining
8 DSC and DWI, Prager *et al.* analyzed 68 HGG patients with 39% MGMT promoter
9 methylation and showed that the sensitivity and specificity of predicting TP were 93% and
10 83%, respectively [77]. In a retrospective study, Park *et al.* analyzed a volume-weighted
11 voxel-based multiparametric clustering (VVMC) method to distinguish PsP and TP in 162
12 GBM patients (108 in the training set and 54 in the test set; 58% PsP) vs single parametric
13 methods (ADC and CBV). In the entire population, VVMC was significantly improved in
14 differentiating TP and PsP compared with any single parameter, with a sensitivity, specificity,
15 and accuracy varying from 87% to 91% for the three parameters [118]. Seeger *et al.*, in a
16 study including 40 HGG patients, demonstrated that the combination of DCE and DCS
17 perfusion techniques led to an increase in sensitivity and accuracy. ASL could improve the
18 accuracy but not the diagnostic performance of the preexisting combination of DCE and DSC.
19 However, the best multiparametric approach was perfusion MRI and MRS, with an accuracy
20 of 90%, a sensitivity of 83%, and a specificity of 100% [92]. Yoon *et al.* studied DWI, DSC,
21 and DCE parameters in 75 GBM patients presenting with enlarged contrast-enhanced lesions
22 one month after CRT, and 55% had MGMT promoter methylation. In patients with MGMT
23 promoter methylation, the probability of PsP was 96% when the CBV90 value was <4.02 and
24 90% when ADC10 was >0.94. The results suggested that MRI parameters were stronger

1 predictors of PsP when the MGMT promoter was methylated than when it was unmethylated,
2 and DSC had the highest accuracy for PsP [119].

3 **5.5.Others modalities**

4 After CRT, patients treated for GBM are prone to blood-brain barrier disruption, so the rCBV
5 can be underestimated when gadolinium-based contrast agents are used. Ferumoxytol is a
6 very small supramagnetic iron oxide nanoparticle (30 nm) that can be a relevant substitute
7 because of its potential to act as a blood pool agent shortly after injection [24,120]. In 2011, a
8 pilot study showed a difference between ferumoxytol rCBV and gadoteridol rCBV values
9 ($p=0.002$) in the TP group but not in the PsP group ($p=0.9$) [98]. In 2013, the same authors
10 reported significantly improved survival in patients with rCBV values ≤ 1.75 ($p=0.001$) using
11 ferumoxytol as a prognostic biomarker in differentiating TP from PsP and predicting survival
12 in GBM patients who did not require contrast agent leakage correction [121]. Other authors
13 proposed ferumoxytol as a gadolinium contrast mismatch ratio for PsP biomarkers [122].

14 Ma *et al.* analyzed 32 patients with gliomas and reported the use of 3T using amide proton
15 transfer-weighted (APTW) imaging features for the differentiation between PsP and TP.
16 $APTW_{\text{mean}}$ and $APTW_{\text{max}}$ signal intensities were higher in the TP group than in the PsP
17 group (2.75% vs 1.56%; $p < 0.001$ and 3.29% vs 1.95%; $p < 0.001$). The respective
18 $APTW_{\text{mean}}$ and $APTW_{\text{max}}$ thresholds for predicting TP were 2.42% (sensitivity of 85% and
19 specificity of 100%) and 2.54% (sensitivity of 95% and specificity of 92%) [123].

20 Tsien *et al.* proposed using parametric response mapping (PRM) in 27 HGG patients. PRM is
21 a voxel-based imaging method applied to perfusion maps to quantify early hemodynamic
22 alterations after treatment. It can measure the difference between serial rCBV maps for each
23 voxel. $P\ PRM_{\text{rCBV}}$ was significantly different between PsP and TP ($p < 0.001$) and could be
24 considered a potential biomarker to distinguish TP from PsP [104].

1 Perfusion MRI-fractional tumor burden (pMRI-FTB) was correlated most strongly with
2 histologic tumor fraction when compared to other metrics and could be a promising TP
3 biomarker [96].

4 **6. Magnetic Resonance Spectroscopy (MRS)**

5 Both PsP and TP may demonstrate neuronal loss or dysfunction (low NAA), abnormal
6 cellular membrane (high Cho), or anaerobic metabolism (high Lac and Lip) [29]. A meta-
7 analysis of 18 articles and 455 glioma patients showed that MRS alone had a moderate impact
8 on the diagnosis of TP, and a Cho/Cr ratio threshold ranging from 1.05 to 2.60 had a
9 sensitivity and specificity of 83%, respectively, and a Cho/NAA ratio threshold ranging from
10 0.88 to 1.90 had a sensitivity and specificity of 88% and 86%, respectively. Consequently, the
11 authors recommended the combination of MRS with advanced imaging technologies [124].

12 MRS can be effective in distinguishing PsP and TP [29,125,126]. In the Zeng *et al.* study of
13 55 HGG patients, MRS correctly classified 85% of patients in both the TP and PsP groups
14 [74]. Table 4 summarizes the literature data concerning metabolite ratios of MRS [68,74–
15 76,79–81,92,93,127–131]. Elias *et al.* demonstrated the ability of nonnormalized Cho/NAA
16 and NAA/Cr ratios to identify TP with sensitivity, specificity, PPV, and NPV of 86%, 90%,
17 93%, and 82% and 84%, 93%, 70%, and 82%, respectively. The normalized Cho/NAA ratio
18 offered a sensitivity, specificity, PPV, and NPV of 73%, 40%, 65%, and 50%, respectively, in
19 a study of 27 primary brain tumor patients [132].

20 Other authors studied the effect of the combination of different imaging modalities to improve
21 PsP identification. Fink *et al.* compared the capacity of multivoxel MRS, single voxel MRS,
22 DSC, and DWI to diagnose TP in 38 glioma patients. The authors suggested that single-voxel
23 MRS was inadequate and that multivoxel MRS should be used to differentiate TP and
24 radiation injuries. The authors proposed a multivoxel Cho/Cr peak area ≥ 1.54 for a sensitivity,
25 specificity, PPV, NPV, and accuracy of 96%, 83%, 96%, 83%, and 93%, respectively, and a

1 multivoxel Cho/NAA peak height ≥ 1.05 for a sensitivity, specificity, PPV, NPV, and
2 accuracy of 91%, 83%, 95%, 71%, and 90%, respectively [76]. The conjunction of the
3 metabolite ratios of MRS and ADC of DWI showed that 96% of patients were classified into
4 the correct group. The sensitivity, specificity, and diagnostic accuracy of 3D-MRS were 94%,
5 100% and 96%, respectively [74]. Di Costanzo *et al.* studied the combination of MRS,
6 conventional MRI, DWI, and perfusion MRI in 29 HGG patients. The discrimination
7 accuracy was 79% when considering only Cho/Cr, 86% when considering Cho/Cr and ADC,
8 90% when considering Cho/Cr and rCBV, and 97% when considering Cho/Cr, ADC, and
9 rCBV [133]. Matsusue *et al.* demonstrated, in 15 glioma patients, a threshold of 1.30 for the
10 ADC ratio, 2.10 for the rCBV ratio, 1.29 for the Cho/Cr ratio, and 1.06 for the Cho/NAA ratio
11 for accuracies of 87%, 87%, and 85%, respectively. The accuracy of distinguishing TP from
12 PsP reached 93% by combining DWI, DSC, and MRS [134]. A comparison of conventional
13 MRI to MRS, perfusion MRI and FDG-PET in 24 glioma patients (11 GBM) showed that the
14 PPVs were 50%, 92%, 75%, and 100%, respectively. The NPVs for MRS, perfusion MRI,
15 and FDG-PET were 100%, 61%, and 100%, respectively, demonstrating the superiority of
16 MRS and perfusion MRI vs FDG-PET for diagnosing TP [135]. Verma *et al.* proposed 3D
17 echo-planar spectroscopy to differentiate PsP and TP [136].
18 Because of user variability to determine the regions of interest and lower spatial resolution,
19 MRS-induced uncertainty, and lack of reproducibility, definition and validation of the
20 thresholds to diagnose PsP and TP is necessary in clinical practice and clinical trials. The
21 limitations of MRS could be the voxel sizes combined with partial volume effects, time
22 acquisition, signal contamination, and the various metabolite ratios used in studies
23 [42,68,74,92,93,133].

24 **7. Positron-Emission-Tomography (PET)**

1 The most common and available PET modality is fluorodeoxyglucose (FDG)-PET, which
2 often has standardized image acquisition but is limited for distinguishing PsP and TP. Novel
3 tracers with lower background brain activity were studied to evaluate TP [137]. Some authors
4 found that amino acid tracers such as methyl-L-methionine (MET), fluoroethyl-L-tyrosine
5 (FET) or fluoro-L-dopa (FDOPA) had higher diagnostic accuracy than conventional and
6 advanced MRI in the differentiation of TP and PsP [6]. The European Association of Nuclear
7 Medicine (EANM), the Society of Nuclear Medicine and Molecular Imaging (SNMMI), the
8 European Association of Neurooncology (EANO), and the Working Group for Response
9 Assessment in Neurooncology with PET (PET-RANO) published guidelines for FDG, MET,
10 FET and FDOPA-PET [138]. The PET images could be matched with contrast-enhanced T1
11 and T2/FLAIR MRI images for interpretation [139–141]. The different PET tracers are
12 summarized in Table 5.

13 Standardization of the methodology and analytical approaches is needed to improve
14 comparability and harmonize practices [142].

15 **7.1.2-Deoxy-2-[fluorine-18]fluoro-D-glucose positron emission tomography (¹⁸F-FDG** 16 **PET)**

17 Although FDG-PET has already been validated to distinguish PsP and TP [28,45], it has some
18 limitations in the assessment of TP [27,70,137,143–149]. Similar to GBM progression, which
19 demonstrates increased glucose metabolism, radiation injury can also demonstrate increased
20 FDG uptake [150]. Methods to define a cutoff standardized uptake value (SUV) were
21 unreliable because the relative glucose uptake and FDG-PET varied widely for tumors and
22 were different for the normal brain [150]. Ricci *et al.* concluded, in a study on 31 primary
23 brain tumor patients, that FDG-PET was not a useful tool for the diagnosis of PsP or TP; a
24 comparison with contralateral white matter provided a sensitivity, specificity, PPV, and NPV
25 for the diagnosis of TP of 86%, 22%, 73% and 50%, respectively, and a comparison with

1 contralateral gray matter provided corresponding values of 73%, 56%, 80%, and 46%,
2 respectively [151]. However, Santra *et al.* demonstrated an overall sensitivity, specificity,
3 PPV, NPV, and accuracy of 50%, 100%, 100%, 40%, and 63%, respectively, for diagnosing
4 TP in a GBM subgroup and concluded that FDG-PET was a highly specific modality for
5 detecting TP [45]. In the Larsen *et al.* study, which included 19 glioma patients (13 GBM),
6 DCE and FDG-PET obtained 81% concordance in the classification of new contrast-enhanced
7 lesions [28]. When FDG-PET was combined with perfusion MRI, DWI, and MRS, the
8 diagnostic accuracy improved [75].
9 Other novel tracers, such as FDOPA, MET, and FET, can be more useful.

10 **7.2.¹⁸F-fluoro-L-dopa positron emission tomography (¹⁸F-FDOPA PET)**

11 FDOPA-PET was useful for complementing the diagnosis of GBM and evaluation of possible
12 progression and detected recurrence earlier than MRI [152–154]. Chen *et al.* compared
13 FDOPA-PET and FDG-PET and concluded that the sensitivity of FDOPA-PET was higher
14 than that of FDG-PET for detecting tumors, but the sensitivity was the same with both
15 methods: sensitivity, specificity, accuracy, PPV, and NPV of 96%, 43%, 83%, 85%, and 75%
16 for FDOPA-PET and 61%, 43%, 57%, 78%, and 25% for FDG-PET, respectively. The
17 authors proposed a threshold of tumor uptake to striatum uptake (T/S) and tumor uptake to
18 normal hemispheric tissue uptake (T/N) of >1.0 and >1.3 for a sensitivity and a specificity of
19 96%/100% and 96%/86%, respectively [152]. Hermann *et al.* showed, in 110 GBM patients,
20 that SUV_{max} , SUV_{mean} , T/N_{max} , T/N_{mean} , T/S_{max} , and T/S_{mean} were significantly higher in GBM
21 patients with TP vs no progression, and the $T/S_{max} \geq 1.0$ threshold had a sensitivity of 84%, a
22 specificity of 62%, and an accuracy of 78% [155]. In another study of 28 glioma patients, the
23 sensitivity, specificity, and accuracy of FDOPA-PET and FDOPA-PET were 48%, 100%, and
24 61% and 100%, 86%, and 96%, respectively, with FDOPA-PET being more sensitive and
25 specific in detecting recurrence [156]. FDOPA-PET and MRI fusion provided anatomical

1 localization precision of abnormal FDOPA-PET activity, and the concordance between both
2 enhancing and nonenhancing lesions on MRI and increased FDOPA-PET uptake was
3 approximately 90%. FDOPA-PET could identify tumors not visible on MRI and was able to
4 distinguish recurrent nonenhancing tumors from other causes of T2 signal changes on MRI
5 [153]. A meta-analysis of 15 articles and 640 patients with primary brain tumors reported that
6 FDOPA-PET was more effective than FET-PET ($p=0.015$) [157], another amino tracer that
7 was used and studied.

8 **7.3.O-(2-[¹⁸F]fluoroethyl) -L-tyrosine positron emission tomography (¹⁸F-FET PET)**

9 Several metrics of FET-PET were identified as imaging biomarkers of TP or PsP. In a
10 retrospective study of 22 GBM patients, the mean and maximum tumor-to-brain ratios
11 (TBR_{mean} and TBR_{max}) obtained using FET-PET were higher in the TP group (2.3 and 2.8)
12 than in the PsP group (1.8 and 1.9) ($p<0.001$), and the mean time to peak (TTP) was shorter in
13 the TP group than in the PsP group ($p=0.05$). The optimal TBR_{max} and TBR_{mean} cutoff values
14 for identifying PsP were 2.3 and 2.0, respectively, with a sensitivity of 100% and 82%, a
15 specificity of 91% and 82%, and an accuracy of 96% and 82%, respectively [158]. In another
16 study of 124 glioma patients (50 GBM), the same authors evaluated static and dynamic FET-
17 PET. The TBR_{max} , TBR_{mean} , and TTP thresholds for identifying TP were 2.3, 2.0, and <45
18 min with sensitivities of 68%, 74%, and 82%; specificities of 100%, 91%, and 73%; and
19 accuracies of 71%, 75%, and 81%, respectively. The combined analysis of TBR_{max} and
20 TBR_{mean} cut-offs and kinetic patterns had a sensitivity of 93%, a specificity of 73%, and an
21 accuracy of 91%, but the combined TBR_{mean} cutoff and TTP cutoff had the best results with a
22 sensitivity of 93%, a specificity of 100%, and an accuracy of 93% [159]. Pauleit *et al.*
23 demonstrated, in a study of 28 glioma patients, that the TBR ratio was an independent
24 significant coefficient for the distinction of tumor progression ($p=0.004$) and reported that the
25 TBR_{mean} was 2.6 in TP vs 1.2 in peritumoral tissue ($p<0.001$). The sensitivity and specificity

1 were 92% and 81%, respectively, with a TBR ratio threshold of 1.6 [160]. Kebir *et al.*
2 analyzed 26 GBM patients, 17 of whom had methylated MGMT promoters and reported that
3 TBR_{max} and TBR_{mean} were significantly higher in TP patients than in PsP patients (2.4 vs 1.5,
4 $p=0.003$ and 2.1 vs 1.5, $p=0.012$, respectively) and that TTP was lower in the TP group (25
5 min vs 40 min, $p<0.001$). A TBR_{max} threshold of 1.9 showed a sensitivity, specificity, and
6 accuracy of 84%, 86%, and 85%, respectively [161]. Mihovilovic *et al.* proposed a TBR_{max}
7 threshold of 3.52 with an accuracy of 86% for late PsP [162]. The
8 EANM/SNMMI/EANO/RANO groups recommended the use of FET-PET with a TBR_{max}
9 threshold of 2.3 to differentiate early PsP and TP and a TBR_{max} and TBR_{mean} threshold of 1.9
10 to differentiate late PsP and TP [138].

11 Popperl *et al.* studied 53 glioma patients (27 GBM) and showed that SUV_{max} was superior in
12 cases of TP, and an SUV_{max} threshold of 2.2 had the best differentiation between TP and
13 treatment-related changes. The $SUV_{max}/background$ (BG) ratio threshold had a discriminatory
14 power of 100%. There was also a correlation between the SUV_{max} value and the tumor grade,
15 with high values for high grades [163]. Mehrkens *et al.* showed, in a study that included 31
16 gliomas (8 GBM), that the PPV of FET-PET was 84% for identifying TP with an SUV_{max}/BG
17 ratio of >2.0 [164]. In a pilot study of 14 HGGs with 86% MGMT promoter methylation (11
18 GBM), Kebir *et al.* suggested that textural FET-PET features were more predictive of PsP
19 ($p=0.041$) than the maximum tumor-to-normal brain ratio (TNR_{max}) at an optimal cutoff of
20 2.1 ($p=0.07$) with a sensitivity, specificity, PPV, and NPV of 90%, 75%, 90%, and 75% and
21 70%, 100%, 100%, and 57%, respectively [165].

22 Compared to conventional MRI, FET-PET was significantly more accurate ($p<0.01$) [166].
23 The adjunction of FET-PET to MRI significantly improved the identification of TP with a
24 sensitivity and specificity of 93% and 94%, respectively [160]. The combination of FET-PET
25 and ADC increased the accuracy from 69% to 89% for the differentiation of TP and PsP [167]

1 Compared to MET-PET, FET-PET provided a comparable ability to differentiate treatment-
2 related changes from TP and to delineate the gross target volume (GTV) of tumors with a
3 sensitivity of 91% and specificity of 100% for both tracers [168].

4 **7.4.¹¹C-methyl-L-methionine positron emission tomography (¹¹C-MET PET)**

5 Many studies have demonstrated the use of MET-PET for the management of gliomas. The
6 sensitivity, specificity, and accuracy for detecting TP with MET-PET were 100%, 60%, and
7 82%, respectively [169]. The intensity of MET uptake is associated with the grade of gliomas,
8 so high uptake is associated with poor survival time, indicating MET uptake is a prognostic
9 factor [70,170]. Several studies reported that mean T/N ratio was significantly higher in TP:
10 4.0 vs 1.8 [171], 4.3 vs 1.8 [172], 2.18 vs 1.49 (p<0.01) [130], 2.69 vs 1.01 (p=0.06) [173],
11 1.89 vs 1.44 (p=0.0079) [174], and 2.38 vs 1.04 [93]. The maximum L/N was 2.62 vs 2.11
12 (p=0.052) [174]. A T/N ratio threshold of 2 had a sensitivity of 86% and specificity of 100%
13 [130], and a T/N ratio cutoff of >1.9 had a sensitivity of 95% and specificity of 89% [173].
14 The SUV_{max} (2.89 vs 1.49 [93] and 3.19 vs 2.66 (p=0.036) [174]) and SUV_{mean} (2.65 vs 1.28
15 [93] and 2.31 vs 1.82 (p=0.017) [174]) were both higher in TP patients, and the SUV_{lesion/BG}
16 ratio was also higher in the TP group (2.79 and 1.53) (p<0.05) [175]. In the Garcia *et al.* study
17 of 30 HGG patients, the sensitivity and specificity were 90% and 100%, respectively, at an
18 SUV/BG threshold of 2.35 [175]. Kim *et al.* studied 10 HGG patients (5 GBM) and showed a
19 maximal lesion uptake to maximal contralateral cerebral white matter uptake ratio (L/R_{max})
20 ratio of 2.64 with a sensitivity and specificity of 75% and 100%, respectively [99]. Terakawa
21 *et al.* determined that L/N_{mean} was the most informative index, and an L/N_{mean} cutoff of 1.58
22 had a sensitivity and specificity of 75% and 75%, respectively [174].

23 Some authors did not demonstrate the use of MET-PET for the differentiation between TP
24 and treatment-related changes. Analyzing MET uptake in lesions and in four specific regions
25 (around the lesion, in the contralateral frontal lobe, in the contralateral area, and in the

1 contralateral cerebellar cortex), MET-PET failed to differentiate treatment-related changes
2 from TP with no significant differences in quantitative or qualitative assessments [176]. No
3 significant differences were reported between treatment-related changes and TP patients in
4 the T/N_{mean} ratio of 1.31 vs 1.87 [169], L/R_{max} ratio of 2.07 vs 3.33; $p=0.257$ [99], and
5 SUV_{mean} of 1.81 vs 2.44 [169].

6 Compared to FDG-PET, MET-PET was superior to FDG-PET for the detection of tumor
7 recurrence with a sensitivity, specificity, and accuracy of 96%, 87%, and 94% and 46%,
8 100%, and 58%, respectively [177]. The FDG-PET and MET-PET combination provided the
9 highest accuracy ($p=0.003$), with an accuracy, sensitivity, and specificity of 83%, 95%, and
10 60%, respectively [178]. With a T/N cutoff of >0.75 , FDG had a sensitivity and specificity of
11 81% and 89%, respectively, for identifying recurrence, whereas at a T/N cutoff of >1.9 , MET
12 had a sensitivity and specificity of 95% and 89%, respectively, for identifying recurrence
13 [173].

14 Compared to advanced MRI, MET-PET was more sensitive for diagnosing TP with a
15 sensitivity, specificity, and accuracy of 95%, 80%, and 90%, respectively, whereas advanced
16 MRI was more specific, with a sensitivity, specificity, and accuracy of 84%, 90%, and 86%,
17 respectively [93]. Dandois *et al.* reported that perfusion MRI and MET PET both assisted in
18 diagnosing TP in 28 HGG patients (14 GBM). Of 33 combined MRI and PET studies, 31
19 matched perfectly, and rCBV had equal performance with MET-PET [179]. Another study
20 reported that perfusion MRI with rCBV was superior to both MET-PET and FDG-PET for the
21 differentiation between treatment-related changes and TP [99]. Deuschl *et al.* studied 50
22 glioma patients and proposed a combined use of MRI and PET with hybrid MET-PET/MRI to
23 differentiate treatment-related changes from TP. The sensitivity, specificity, accuracy, and
24 PPV were 86%, 71%, 82%, and 89% for MRI alone, 97%, 74%, 88%, and 86% for MET-
25 PET, and 97%, 93%, 96%, and 97% for MET-PET/MRI, respectively. There was a significant

1 difference between MET-PET/MRI and MRI ($p=0.008$) but no differences between MET-
2 PET and MRI alone ($p=0.021$) or MET-PET/MRI and MET-PET alone ($p=1.000$) [180].

3 **7.5.3'-deoxy-3'[(18)F]-fluorothymidine positron emission tomography (¹⁸F-FLT** 4 **PET)**

5 According to different studies, FLT can assist with glioma detection and grading
6 characterization because its uptake in the normal brain is low, the image contrast is significant
7 [181], and FLT uptake correlates with the Ki67 index [182–185]. It represents a noninvasive
8 method to potentially predict disease progression and response to therapy in gliomas
9 [186,187]. In Choi *et al.*, FLT uptake was correlated with the Ki67 index ($p=0.007$), and
10 changes in FLT uptake were associated with response to therapy [185]. However, FLT uptake
11 depended on blood-brain barrier disruption, which impacted its efficiency in clinical
12 applications [188]. Muzi *et al.* proposed a kinetic analysis of FLT in 12 patients with primary
13 brain tumors that quantified FLT uptake and analyzing blood-brain barrier disruption and
14 retention in tumor tissue as a result of metabolic trapping of FLT nucleotides to separate
15 transport effects from tissue retention. They produced a parametric image map of blood-to-
16 tissue transport (K1) and metabolic flux (KFLT). When the blood-brain barrier broke down,
17 transport dominated FLT uptake, but when the blood brain barrier was intact, transport was
18 limited, and FLT-PET was inefficient. The authors concluded that FLT was not the best tracer
19 for necrosis or nonenhancing lesions [189]. In another study of 19 glioma patients (4 GBM),
20 K1, KFLT, and phosphorylation (K3) were significantly different between TP and treatment-
21 related changes ($p<0.0001$, $p=0.0009$, and $p=0.0012$, respectively) when analyzed using the t-
22 test, but when the Wilcoxon test was used, only KFLT and K3 demonstrated significant
23 differences. The authors suggested that FLT-PET was promising for the diagnosis of TP with
24 rigorous dynamic parameters [190].

1 Some authors demonstrated that FLT-PET had no use in the discrimination of PsP vs TP. In
2 the den Hollander *et al.* study evaluating 28 GBM and two gliosarcomas, no difference in
3 SUV_{max} was found between patients with TP and patients with PsP [191]. In a more recent
4 prospective study of 24 GBM patients, the SUV_{max} and T/N ratio did not differ significantly
5 between the PsP and TP groups (1.41 vs 1.28, p=0.699, and 4.03 vs 3.59, p=0.699,
6 respectively) [192]. Compared to FDG-PET, FLT-PET was not more reliable than FDG-PET
7 for the distinction between TP and treatment-related changes, with a sensitivity and
8 specificity varying from 73% to 91% and 75% vs from 91% to 100% and 75%, respectively
9 [193].

10 **7.6.Others PET tracers**

11 Other PET tracers were evaluated in the literature. ¹¹C-choline [194], ¹¹C-methyl-L-
12 tryptophan (MLT) [195], ¹⁸F-fluoromisonidazole (FMISO) [196,197], ¹⁸F-
13 fluoromethylcholine (FCho) [198], and 4-borono-2-¹⁸F-fluoro-phenylalanine (¹⁸F-FBPA)
14 [199,200] could be useful for the differentiation between PsP and TP, but studies are currently
15 too rare to promote their use.

16 **7.7.Single photon-emission computed tomography (SPECT)**

17 In a meta-analysis of 893 patients with gliomas, SPECT was able to differentiate PsP and TP
18 with a sensitivity of 89% and a specificity of 87% [201]. Some SPECT tracers were studied in
19 the literature.

20 In a retrospective study of 19 HGG patients, thallium 201 (²⁰¹Tl)-SPECT had better
21 sensitivity, specificity, PPV, and NPV than conventional MRI (84%, 100%, 100%, and 57%
22 vs 65%, 75%, 92%, and 33%, respectively) and a higher TP diagnostic accuracy (86% vs
23 67%) [202]. Caresia *et al.* found that the sensitivity, specificity, and accuracy of ²⁰¹Tl-SPECT
24 were 100% [203]. Vos *et al.* estimated that the sensitivity and specificity of ²⁰¹Tl-SPECT
25 ranged from 43% to 100% and from 25% to 100%, respectively. However, the poor

1 methodological quality and small sample sizes of the included studies impeded conclusions
2 [204]. Compared to FDG-PET, ^{201}Tl -SPECT had a higher sensitivity but a lower specificity
3 and was better at excluding TP [205].

4 Sestamibi technetium 99m ($^{99\text{m}}\text{Tc}$ -MIBI) SPECT had a sensitivity, specificity, and accuracy
5 of 89%, 83%, and 87%, respectively, for diagnosing TP [206]. Compared with MRS, $^{99\text{m}}\text{Tc}$ -
6 MIBI-SPECT had a sensitivity, specificity, accuracy, PPV, and NPV of 90%, 100%, 93%,
7 100%, and 83%, respectively, and the combination of $^{99\text{m}}\text{Tc}$ -MIBI-SPECT and MRS had a
8 sensitivity, specificity, accuracy, PPV, and NPV of 95%, 100%, 97%, 100%, and 91%,
9 respectively [207].

10 Plotkin *et al.* investigated 123-iodine-a-methyl tyrosine (^{123}I -IMT) SPECT and single voxel
11 MRS in 25 glioma patients (10 GBM) and reported that although ^{123}I -IMT SPECT had a trend
12 of better performance than single voxel MRS, no significant differences were observed in the
13 accuracy, sensitivity, and specificity between the two modalities ($p>0.05$) for diagnosing TP
14 [131].

15 Amin *et al.* compared technetium-99m-dimercaptosuccinic acid ($^{99\text{m}}\text{Tc}$ (V)DMSA)-SPECT
16 and MRS in 24 patients with primary brain tumors (7 GBM) treated with surgery and RCT
17 and concluded that $^{99\text{m}}\text{Tc}$ (V)DMSA-SPECT was more effective than MRS for diagnosing TP
18 with a sensitivity, specificity, accuracy, PPV, and NPV of 89%, 100%, 92%, 75%, and 100%,
19 respectively [208].

20 In 2007, Alexiou *et al.* studied $^{99\text{m}}\text{Tc}$ -tetrofosmin ($^{99\text{m}}\text{Tc}$ -TF) SPECT in 11 patients with
21 glioma (4 GBM) and proposed a lesion uptake to normal brain tissue uptake ratio (L/N)
22 threshold value of 4.76 for diagnosing TP [209]. In 2014, the same authors compared DTI,
23 DSC, and $^{99\text{m}}\text{Tc}$ -TF-SPECT in a prospective study of 30 HGG patients and reported an L/N
24 threshold value of 4 with 100% sensitivity and 100% specificity [78].

1 A comparison of ^{99m}Tc-methionine-SPECT, FDG-PET, and conventional MRI demonstrated
2 that the specificity of ^{99m}Tc-MET-SPECT was significantly higher than the specificity of
3 conventional MRI (p<0.0001) but not the specificity of FDG-PET (p=0.36). No significant
4 difference in sensitivity or accuracy was observed among [210].

5 ^{99m}Tc-glucoheptonate (GHA) SPECT is a low-cost radiopharmaceutical agent that can be
6 strongly recommended for detecting residual tumors after surgery/radiotherapy and
7 progression [211].

8 ^{99m}TcMDM (bis-methionine-DTPA) SPECT had a comparable sensitivity and specificity to
9 DSC (92% and 79% for MDM SPECT and 92% and 71% for DSC MRI) [212].

10 **8. True progression vs pseudoprogression**

11 Differentiating PsP from TP remains a persistent challenge in routine clinical practice. Some
12 radiological techniques with variable sensitivity, specificity and accuracy are available to help
13 clinicians (Table 6). According to this literature review, Figure 1 proposes a decision diagram
14 to orient clinical decision-making and assist with the distinction between PsP and TP. The
15 order of radiological imaging features proposed was based on the specificity and PPV of the
16 different radiological examinations in the literature. Based on the RANO and modified
17 RANO criteria for the response assessment, conventional MRI results associated with clinical
18 evaluation and corticosteroid use were the three conventional and routinely used criteria to
19 differentiate PsP and TP [34,37]. In addition to those criteria, MGMT promoter methylation
20 status could help inform the diagnosis. Indeed, some authors identified MGMT promoter
21 methylation as a molecular marker and found that approximately two-thirds of MGMT-
22 methylated tumors exhibited PsP [15,23,112,119,158,213–217], and an MRI suggesting
23 progression was associated with a 3.5-fold increased risk of having PsP rather than TP [216].
24 In the case of inconclusive results, additional radiological parameters could help clinicians
25 diagnose TP versus PsP. Traditionally, the first step of those complementary exams consisted

1 of diffusion and perfusion MRI. According to the literature, the mean ADC value, ADC ratio
2 and mean rCBV suggested TP if they showed values of <1.28-1.33, <1.40-1.55 and >1.82-
3 3.01, respectively (Tables 2 and 3, Figure 1). In case of remaining PsP doubt, MRS and PET
4 scans could provide supplementary information as a second step. The proposed MRS ratios to
5 differentiate PsP and TP were Cho/NAA and Cho/Cr, with Cho/NAA <1.47-2.11 and Cho/Cr
6 <0.82-2.25 indicating PsP according to the literature data (Table 4, Figure 1). PET scan
7 evaluation offers numerous metabolic tracers with higher diagnostic accuracy than FDG, such
8 as MET, FET or FDOPA. Finally, this review demonstrated that multiparametric imaging was
9 the best way to differentiate PsP from TP. However, some additional effort and research are
10 needed to increase the accuracy of the different modalities, and machine learning could
11 resolve this issue.

12 Radiomic features combined with clinical and genomic features could improve the diagnostic
13 differentiation between PsP and TP [218–220]. Some authors developed machine learning
14 models to improve PsP versus TP differentiation. Hu *et al.* analyzed multimodal MRI data
15 from 31 GBM patients (15 with TP and 16 with PsP) and developed a machine learning
16 algorithm to identify PsP versus TP with a sensitivity of 89.9% and a specificity of 93.7%,
17 respectively [101]. Elshafeey *et al.* retrospectively demonstrated an accuracy of 90.8% for
18 perfusion MRI data coupled with a support vector machine as a radiomic model to distinguish
19 PsP and TP by analyzing data from 98 GBM patients [218]. Bacchi *et al.* conducted a pilot
20 study in 55 HGG patients combining MRI sequences and identified that deep learning models
21 based on DWI+FLAIR had higher accuracy (0.82), DWI+FLAIR and ADC had higher
22 sensitivity (1.00) and DWI+FLAIR had higher specificity (1.00) [221]. Gao *et al.* developed a
23 deep learning methodology using a deep neural network independent of handcrafting and
24 segmentation for the automated distinction between PsP and TP based on routine multimodal
25 MRI with a retrospective study of 146 GBM patients (66% TP and 34% after pathological

1 examination). The sensitivity, specificity and accuracy were 0.96, 0.80 and 0.90, respectively,
2 which were significantly higher than those associated with neurosurgeon interpretation [222].
3 Bani-Sadr *et al.* showed that MGMT promoter status improved a machine learning model
4 based on conventional radiomics MRI [223]. Advances in neurooncology radiomics were
5 supported by available data from The Cancer Imaging Archive (TCIA) [224] and incorporated
6 tumor segmentation, tumor classification, treatment response assessment, prognostication and
7 therapeutic decisions [225]. The differentiation of PsP from TP was crucial, and machine
8 learning approaches incorporating multiple MRI data possibly associated with other imaging
9 modality data [226], clinical data and genomics [223] seemed to increase this challenging
10 task, even if additional studies with large patient samples were needed [62,225,227–230].
11 Currently, the only way to diagnose PsP versus TP with certainty is a histopathological
12 analysis. However, neurosurgery and neurobiopsy have associated morbidity and mortality,
13 and the use of a noninvasive method to discern PsP and TP with fewer adverse effects seems
14 essential. Compared to surgery, gadolinium-based contrast agents used for MR imaging have
15 fewer and less common issues [231] such as the rare risk of nephrogenic systemic fibrosis
16 [232], deposition/retention of gadolinium in organs [233,234], environmental contamination
17 [235,236], post-contrast acute kidney injury, and allergic reaction [237]. However,
18 neurosurgery complications are numerous and more frequent, especially in the elderly, such
19 as postoperative hemorrhages (intraparenchymal, subdural and epidural), cerebrospinal fluid
20 leakage, pulmonary embolism, new postoperative neurological deficits, epilepsy, weakness,
21 and classical perioperative complications [238–245]. GBM exhibited high heterogeneity,
22 which could not be reflected in biopsy. Neurobiopsy could fail TP vs. PsP diagnosis, as they
23 are noninformative in 3% to 6% of cases with complications such as brain hemorrhage (5% to
24 9% cases), infection (<1% cases), and neurological deficit (2% to 6% cases), and neurobiopsy
25 is associated with a mortality rate from 0.4% to 2% [246–260].

1 Because biopsy, an invasive procedure, may not reflect the complete molecular features of the
2 evolving GBM tumor (60% to 70% of GBM mutations are not present across all regions of a
3 tumor [261]) and the distinction between PsP and TP is not always possible; therefore,
4 radiological imaging and blood-based biomarkers could be interesting, as they improve
5 specificity and decrease morbidity and mortality [262]. Some authors have shown that liquid
6 biopsies from blood, cerebrospinal fluid (CSF) or urinary fluid containing circulating
7 biomarkers are noninvasive or minimally invasive, quick and inexpensive methods that could
8 be more representative of the entire tumor and its heterogeneity [262,263] and useful for
9 GBM diagnosis and treatment monitoring [263–267].

10 Circulating biomarkers are represented by circulating tumor stem cells [268,269], circulating
11 cell-free nucleic acids [263] or circulating tumor cell clusters [270] with circulating tumor
12 cells (CTCs), circulating tumor DNA (ctDNA), cell-free DNA or extracellular vesicles (EVs)
13 [271–274]. These biomarkers could help to guide the diagnosis between PsP and TP using a
14 genomic analysis. Raza *et al.* analyzed 58 studies and 1853 patients and identified 133
15 biomarkers of GBM and 38 biomarkers for the differentiation of TP versus PsP [275]. CTCs
16 were described to contribute to tumorigenesis and recurrence in GBM [269,276]. Even if
17 CTCs are rare and challenging to isolate, with 20-82% sensitivity in blood [262], they can
18 provide information on protein, DNA or RNA levels, and guide therapeutic decisions
19 [277,278]. The isolation of CTCs [279] could be useful during follow-up [262,279–282] as a
20 complement to radiographic features [283]. However, the molecular information obtained
21 may not be representative of the entire GBM [265]. EVs (exosomes or microvesicles) are not
22 exclusively released from tumor cells. EVs contain nucleic acid biomarkers and protein
23 biomarkers and participate in angiogenesis, resistance to apoptosis, and proliferation
24 [262,267,278,284–289]. The authors showed that the EV detection sensitivity and specificity
25 in blood and CSF were 28-91.7% and 86-100% and 61-87% and 93-100%, respectively [290].

1 EVs have a very short half-life, which could reflect rapid changes in GBM biology [262]. The
2 authors also reported that IDH1 mutation, EGFR amplification or BRAF and KRAS mutation
3 could guide GBM diagnosis, glioma grading and assist in monitoring response assessment
4 [291]. EV analysis could be promising in the differentiation between PsP and TP [292]. The
5 authors demonstrated higher EV plasma levels in GBM patients, which decreased after
6 surgery and increased in the case of progression [293]. Koch *et al.* concluded that
7 microvesicle counts were significantly lower in PsP patients than in TP patients ($p=0.014$) in
8 a prospective study of 11 GBM patients [292]. Ct DNA is easier to detect, particularly in
9 CSF, but it has a short half-life [262,265]. The authors reported a sensitivity and specificity of
10 ctDNA detection in blood and CSF of 50-60% and 100% and 58-87% and 97-100%,
11 respectively [290]. CtDNA allows the identification of various mutations, such as IDH1
12 mutation, PTEN mutation, MGMT methylation or EGFR amplification [278,290,294]. The
13 levels of ctDNA were correlated with disease stage, and ctDNA allowed response assessment
14 evaluation [295]. Circulating miRNAs derived from CSF or blood [290] were studied as
15 biomarkers of GBM [262,272,296–300]; they were correlated with tumor grading [301,302],
16 tumor volume [303], treatment response [302,304] with restored levels after CRT [302],
17 conferred chemoresistance [304], prognosis [301] and survival [301]. Swellan *et al.*
18 concluded that miR-221 and miR-222 were increased in progressive disease versus stable
19 disease, complete response or partial response to treatment [305]. Circulating microRNA
20 analysis could be interesting for identifying TP versus PsP because miRNA accurately
21 identifies cancer tissue [175,262,275]. A prospective study of 91 gliomas showed that miRNA
22 levels did not increase in cases of PsP compared to TP [303]. A literature review showed that
23 circulating biomarkers could provide GBM management and facilitate initial and recurrence
24 diagnosis, tumor response assessment, genomic and molecular evolution tracking and PsP
25 identification [306]. Implementation in clinical practice could improve personalized medicine

1 in terms of diagnosis, treatment, and follow-up. However, limitations of liquid biopsy persist
2 and the lack of reproducibility, consensus and standardization of biological fluid type (blood,
3 serum, CSF, urinary), nucleic acid type, and analytical technique (extraction methods,
4 measurement methods) remain [263,301,302]. Many studies were in vitro and not in vivo, and
5 cohort sizes were limited [265,287]. Additional studies seem necessary before clinical use.

6 **9. Conclusion**

7 PsP doubt is a common situation in clinical routines, and clinicians need uniform and
8 standardized criteria to confirm this diagnosis. The use of advanced radiological imaging and
9 imaging biomarkers is promising in this context and provides pathophysiological information.
10 This report demonstrated the superiority of advanced MRI techniques and PET for the
11 diagnosis of PsP, but efforts to create uniform practices and protocols are necessary. It is
12 essential that imaging is available, accessible, reproducible, and cost-effective. This review of
13 the literature indicates that there was no rigorous methodology to guide researchers and
14 provide comparable results based on the large number of parameter cutoff values, different
15 imaging protocols, small sample sizes, different population characteristics, and a lack of study
16 reproducibility. The variability in the extent of isotopes for TEP and SPECT and sequences
17 for MRI, multiplied by the large numbers of metrics evaluated, is significant. Algorithms
18 proposed by artificial intelligence and radiomics were used to analyze the results and improve
19 the usefulness of the data.

20 **Conflict of interest statement**

21 None

22 **Funding source**

23 This research did not receive any specific grant from funding agencies in the public,
24 commercial, or not-for-profit sectors.

25 **Abbreviations**

- 1 **ADC:** Apparent Diffusion Coefficient
- 2 **ASL:** Arterial Spin Labeling
- 3 **BPTI:** International Brain Tumor Imaging
- 4 **CBF:** Cerebral Blood Flow
- 5 **CBV:** Cerebral Blood Volume
- 6 **CE:** Contrast Enhancement
- 7 **CEL:** contrast enhanced lesion
- 8 **CRT:** Chemoradiotherapy
- 9 **CT:** Computed Tomography
- 10 **DCE:** Dynamic Contrast Enhanced
- 11 **DSC:** Dynamic Susceptibility Contrast
- 12 **DTI:** Diffusion Tensor Imaging
- 13 **DWI:** Diffusion Weight Imaging
- 14 **FA:** Fractional Anisotropy
- 15 **FDG:** Fluoro-Deoxy-Glucose
- 16 **FDOPA:** Fluoro-L-Dopa
- 17 **FET:** Fluoroethyl-L-Tyrosine
- 18 **FLT:** F-Fluorothymidine
- 19 **FMISO:** F-fluoromisonidazole
- 20 **GBM:** Glioblastoma
- 21 **HGG:** High Grade Glioma
- 22 **K_{ep} :** Transfer constant from the extracellular-extravascular space into the plasma
- 23 **K^{trans} :** Volume Transfer Constant
- 24 **MET:** methyl-L-methionine
- 25 **MRI:** Magnetic Resonance Imaging

- 1 **MRS:** Magnetic Resonance Spectroscopy
- 2 **PET:** Positron Emission Tomography
- 3 **PsP:** Pseudoprogression
- 4 **RT:** Radiotherapy
- 5 **SPECT:** Single Photon Emission Computed Tomography
- 6 **SUV:** Standardized Uptake Value
- 7 **SWI:** Susceptibility-weighted imaging
- 8 **TBR:** Tumor to Brain Ratio
- 9 **TMZ:** Temozolomide
- 10 **TNR:** Tumor-to-Normal brain Ratio
- 11 **TP:** True Progression
- 12 **V_e:** Volume of extravascular-extracellular space
- 13 **V_p:** Vascular plasma volume

References

1. Siegel RL, Miller KD, Jemal A. Cancer statistics, 2020. *CA Cancer J Clin.* 2020;70(1):7–30.
2. Ostrom QT, Gittleman H, Stetson L, Virk SM, Barnholtz-Sloan JS. Epidemiology of gliomas. *Cancer Treat Res.* 2015;163:1–14.
3. Ostrom QT, Gittleman H, Farah P, Ondracek A, Chen Y, Wolinsky Y, et al. CBTRUS statistical report: Primary brain and central nervous system tumors diagnosed in the United States in 2006-2010. *Neuro-Oncol.* 2013 Nov;15 Suppl 2:ii1-56.
4. Ahmed R, Oborski MJ, Hwang M, Lieberman FS, Mountz JM. Malignant gliomas: current perspectives in diagnosis, treatment, and early response assessment using advanced quantitative imaging methods. *Cancer Manag Res.* 2014;6:149–70.
5. Dolecek TA, Propp JM, Stroup NE, Kruchko C. CBTRUS Statistical Report: Primary Brain and Central Nervous System Tumors Diagnosed in the United States in 2005–2009. *Neuro-Oncol.* 2012 Nov 1;14(suppl_5):v1–49.
6. Albert NL, Weller M, Suchorska B, Galldiks N, Soffietti R, Kim MM, et al. Response Assessment in Neuro-Oncology working group and European Association for Neuro-Oncology recommendations for the clinical use of PET imaging in gliomas. *Neuro-Oncol.* 2016;18(9):1199–208.
7. Bleeker FE, Molenaar RJ, Leenstra S. Recent advances in the molecular understanding of glioblastoma. *J Neurooncol.* 2012 May;108(1):11–27.
8. Stupp R, Mason WP, van den Bent MJ, Weller M, Fisher B, Taphoorn MJB, et al. Radiotherapy plus concomitant and adjuvant temozolomide for glioblastoma. *N Engl J Med.* 2005 Mar 10;352(10):987–96.
9. Seystahl K, Wick W, Weller M. Therapeutic options in recurrent glioblastoma--An update. *Crit Rev Oncol Hematol.* 2016 Mar;99:389–408.
10. Tamimi AF, Juweid M. Epidemiology and Outcome of Glioblastoma. In: De Vleeschouwer S, editor. *Glioblastoma* [Internet]. Brisbane (AU): Codon Publications; 2017 [cited 2020 Nov 21]. Available from: <http://www.ncbi.nlm.nih.gov/books/NBK470003/>
11. Hanif F, Muzaffar K, Perveen K, Malhi SM, Simjee SU. Glioblastoma Multiforme: A Review of its Epidemiology and Pathogenesis through Clinical Presentation and Treatment. *Asian Pac J Cancer Prev APJCP.* 2017 01;18(1):3–9.
12. Witthayanuwat S, Pesee M, Supaadirek C, Supakalin N, Thamronganantasakul K, Krusun S. Survival Analysis of Glioblastoma Multiforme. *Asian Pac J Cancer Prev APJCP.* 2018 Sep 26;19(9):2613–7.
13. Stupp R, Hegi ME, Mason WP, van den Bent MJ, Taphoorn MJB, Janzer RC, et al. Effects of radiotherapy with concomitant and adjuvant temozolomide versus radiotherapy alone on survival in glioblastoma in a randomised phase III study: 5-year analysis of the EORTC-NCIC trial. *Lancet Oncol.* 2009 May;10(5):459–66.
14. Tykocki T, Eltayeb M. Ten-year survival in glioblastoma. A systematic review. *J Clin Neurosci Off J Neurosurg Soc Australas.* 2018 Aug;54:7–13.
15. Brandes AA, Franceschi E, Tosoni A, Blatt V, Pession A, Tallini G, et al. MGMT promoter methylation status can predict the incidence and outcome of pseudoprogression after concomitant radiochemotherapy in newly diagnosed glioblastoma patients. *J Clin Oncol Off J Am Soc Clin Oncol.* 2008 May 1;26(13):2192–7.
16. Chamberlain MC, Glantz MJ, Chalmers L, Van Horn A, Sloan AE. Early necrosis following concurrent Temodar and radiotherapy in patients with glioblastoma. *J Neurooncol.* 2007 Mar;82(1):81–3.
17. Taal W, Brandsma D, de Bruin HG, Bromberg JE, Swaak-Kragten AT, Smitt PAES, et al. Incidence of early pseudo-progression in a cohort of malignant glioma patients treated

- with chemoirradiation with temozolomide. *Cancer*. 2008 Jul 15;113(2):405–10.
18. Wick W, Chinot OL, Bendszus M, Mason W, Henriksson R, Saran F, et al. Evaluation of pseudoprogression rates and tumor progression patterns in a phase III trial of bevacizumab plus radiotherapy/temozolomide for newly diagnosed glioblastoma. *Neuro-Oncol*. 2016;18(10):1434–41.
 19. Brandsma D, Stalpers L, Taal W, Sminia P, van den Bent MJ. Clinical features, mechanisms, and management of pseudoprogression in malignant gliomas. *Lancet Oncol*. 2008 May;9(5):453–61.
 20. Rowe LS, Butman JA, Mackey M, Shih JH, Cooley-Zgela T, Ning H, et al. Differentiating pseudoprogression from true progression: analysis of radiographic, biologic, and clinical clues in GBM. *J Neurooncol*. 2018 May 16;
 21. Chaskis C, Neyns B, Michotte A, De Ridder M, Everaert H. Pseudoprogression after radiotherapy with concurrent temozolomide for high-grade glioma: clinical observations and working recommendations. *Surg Neurol*. 2009 Oct;72(4):423–8.
 22. Chang JH, Kim C-Y, Choi BS, Kim YJ, Kim JS, Kim IA. Pseudoprogression and pseudoresponse in the management of high-grade glioma : optimal decision timing according to the response assessment of the neuro-oncology working group. *J Korean Neurosurg Soc*. 2014 Jan;55(1):5–11.
 23. Zikou A, Sioka C, Alexiou GA, Fotopoulos A, Voulgaris S, Argyropoulou MI. Radiation Necrosis, Pseudoprogression, Pseudoresponse, and Tumor Recurrence: Imaging Challenges for the Evaluation of Treated Gliomas. *Contrast Media Mol Imaging*. 2018;2018:6828396.
 24. Nasser M, Gahramanov S, Netto JP, Fu R, Muldoon LL, Varallyay C, et al. Evaluation of pseudoprogression in patients with glioblastoma multiforme using dynamic magnetic resonance imaging with ferumoxytol calls RANO criteria into question. *Neuro-Oncol*. 2014 Aug;16(8):1146–54.
 25. Jefferies S, Burton K, Jones P, Burnet N. Interpretation of Early Imaging after Concurrent Radiotherapy and Temozolomide for Glioblastoma. *Clin Oncol*. 2007 Apr 1;19(3):S33.
 26. Radbruch A, Fladt J, Kickingereeder P, Wiestler B, Nowosielski M, Bäumer P, et al. Pseudoprogression in patients with glioblastoma: clinical relevance despite low incidence. *Neuro-Oncol*. 2015 Jan;17(1):151–9.
 27. Tran DKT, Jensen RL. Treatment-related brain tumor imaging changes: So-called “pseudoprogression” vs. tumor progression: Review and future research opportunities. *Surg Neurol Int*. 2013;4(Suppl 3):S129-135.
 28. Larsen VA, Simonsen HJ, Law I, Larsson HBW, Hansen AE. Evaluation of dynamic contrast-enhanced T1-weighted perfusion MRI in the differentiation of tumor recurrence from radiation necrosis. *Neuroradiology*. 2013 Feb;55(3):361–9.
 29. Hygino da Cruz LC, Rodriguez I, Domingues RC, Gasparetto EL, Sorensen AG. Pseudoprogression and pseudoresponse: imaging challenges in the assessment of posttreatment glioma. *AJNR Am J Neuroradiol*. 2011 Dec;32(11):1978–85.
 30. Jahangiri A, Aghi MK. Pseudoprogression and treatment effect. *Neurosurg Clin N Am*. 2012 Apr;23(2):277–87, viii–ix.
 31. Abbasi AW, Westerlaan HE, Holtman GA, Aden KM, van Laar PJ, van der Hoorn A. Incidence of Tumour Progression and Pseudoprogression in High-Grade Gliomas: a Systematic Review and Meta-Analysis. *Clin Neuroradiol*. 2018 Sep;28(3):401–11.
 32. Thust SC, van den Bent MJ, Smits M. Pseudoprogression of brain tumors. *J Magn Reson Imaging JMRI*. 2018 May 7;
 33. Wen PY, Chang SM, Van den Bent MJ, Vogelbaum MA, Macdonald DR, Lee EQ. Response Assessment in Neuro-Oncology Clinical Trials. *J Clin Oncol Off J Am Soc Clin*

Oncol. 2017 Jul 20;35(21):2439–49.

34. Wen PY, Macdonald DR, Reardon DA, Cloughesy TF, Sorensen AG, Galanis E, et al. Updated response assessment criteria for high-grade gliomas: response assessment in neuro-oncology working group. *J Clin Oncol Off J Am Soc Clin Oncol*. 2010 Apr 10;28(11):1963–72.
35. Macdonald DR, Cascino TL, Schold SC, Cairncross JG. Response criteria for phase II studies of supratentorial malignant glioma. *J Clin Oncol Off J Am Soc Clin Oncol*. 1990 Jul;8(7):1277–80.
36. Ellingson BM, Bendszus M, Boxerman J, Barboriak D, Erickson BJ, Smits M, et al. Consensus recommendations for a standardized Brain Tumor Imaging Protocol in clinical trials. *Neuro-Oncol*. 2015 Sep;17(9):1188–98.
37. Ellingson BM, Wen PY, Cloughesy TF. Modified Criteria for Radiographic Response Assessment in Glioblastoma Clinical Trials. *Neurother J Am Soc Exp Neurother*. 2017;14(2):307–20.
38. Lieberman F. Glioblastoma update: molecular biology, diagnosis, treatment, response assessment, and translational clinical trials. *F1000Research* [Internet]. 2017 Oct 26 [cited 2018 Sep 3];6. Available from: <https://www.ncbi.nlm.nih.gov/pmc/articles/PMC5658706/>
39. Masch WR, Wang PI, Chenevert TL, Junck L, Tsien C, Heth JA, et al. Comparison of Diffusion Tensor Imaging and Magnetic Resonance Perfusion Imaging in Differentiating Recurrent Brain Neoplasm From Radiation Necrosis. *Acad Radiol*. 2016 May;23(5):569–76.
40. Shukla G, Alexander GS, Bakas S, Nikam R, Talekar K, Palmer JD, et al. Advanced magnetic resonance imaging in glioblastoma: a review. *Chin Clin Oncol*. 2017 Aug;6(4):40.
41. Hyare H, Thust S, Rees J. Advanced MRI Techniques in the Monitoring of Treatment of Gliomas. *Curr Treat Options Neurol*. 2017 Mar;19(3):11.
42. van Dijken BRJ, van Laar PJ, Holtman GA, van der Hoorn A. Diagnostic accuracy of magnetic resonance imaging techniques for treatment response evaluation in patients with high-grade glioma, a systematic review and meta-analysis. *Eur Radiol*. 2017 Oct;27(10):4129–44.
43. Neal ML, Trister AD, Ahn S, Baldock A, Bridge CA, Guyman L, et al. Response classification based on a minimal model of glioblastoma growth is prognostic for clinical outcomes and distinguishes progression from pseudoprogression. *Cancer Res*. 2013 May 15;73(10):2976–86.
44. Ellingson BM, Chung C, Pope WB, Boxerman JL, Kaufmann TJ. Pseudoprogression, radionecrosis, inflammation or true tumor progression? challenges associated with glioblastoma response assessment in an evolving therapeutic landscape. *J Neurooncol*. 2017 Sep;134(3):495–504.
45. Santra A, Kumar R, Sharma P, Bal C, Kumar A, Julka PK, et al. F-18 FDG PET-CT in patients with recurrent glioma: comparison with contrast enhanced MRI. *Eur J Radiol*. 2012 Mar;81(3):508–13.
46. https://www.nccn.org/professionals/physician_gls/f_guidelines.asp#n1.
47. Agarwal A, Kumar S, Narang J, Schultz L, Mikkelsen T, Wang S, et al. Morphologic MRI features, diffusion tensor imaging and radiation dosimetric analysis to differentiate pseudo-progression from early tumor progression. *J Neurooncol*. 2013 May;112(3):413–20.
48. Gladwish A, Koh E-S, Hoisak J, Lockwood G, Millar B-A, Mason W, et al. Evaluation of early imaging response criteria in glioblastoma multiforme. *Radiat Oncol Lond Engl*. 2011 Sep 23;6:121.
49. Mullins ME, Barest GD, Schaefer PW, Hochberg FH, Gonzalez RG, Lev MH. Radiation necrosis versus glioma recurrence: conventional MR imaging clues to diagnosis. *AJNR Am J Neuroradiol*. 2005 Sep;26(8):1967–72.
50. Young RJ, Gupta A, Shah AD, Graber JJ, Zhang Z, Shi W, et al. Potential utility of

- conventional MRI signs in diagnosing pseudoprogression in glioblastoma. *Neurology*. 2011 May 31;76(22):1918–24.
51. Kim HS, Goh MJ, Kim N, Choi CG, Kim SJ, Kim JH. Which combination of MR imaging modalities is best for predicting recurrent glioblastoma? Study of diagnostic accuracy and reproducibility. *Radiology*. 2014 Dec;273(3):831–43.
52. Reddy K, Westerly D, Chen C. MRI patterns of T1 enhancing radiation necrosis versus tumour recurrence in high-grade gliomas. *J Med Imaging Radiat Oncol*. 2013 Jun;57(3):349–55.
53. Hansen MR, Pan E, Wilson A, McCreary M, Wang Y, Stanley T, et al. Post-gadolinium 3-dimensional spatial, surface, and structural characteristics of glioblastomas differentiate pseudoprogression from true tumor progression. *J Neurooncol*. 2018 Jun 7;
54. Chen X, Wei X, Zhang Z, Yang R, Zhu Y, Jiang X. Differentiation of true-progression from pseudoprogression in glioblastoma treated with radiation therapy and concomitant temozolomide by GLCM texture analysis of conventional MRI. *Clin Imaging*. 2015 Oct;39(5):775–80.
55. Zaki HS, Jenkinson MD, Du Plessis DG, Smith T, Rainov NG. Vanishing contrast enhancement in malignant glioma after corticosteroid treatment. *Acta Neurochir (Wien)*. 2004 Aug;146(8):841–5.
56. de Groot JF, Fuller G, Kumar AJ, Piao Y, Eterovic K, Ji Y, et al. Tumor invasion after treatment of glioblastoma with bevacizumab: radiographic and pathologic correlation in humans and mice. *Neuro-Oncol*. 2010 Mar;12(3):233–42.
57. Ito-Yamashita T, Nakasu Y, Mitsuya K, Mizokami Y, Namba H. Detection of tumor progression by signal intensity increase on fluid-attenuated inversion recovery magnetic resonance images in the resection cavity of high-grade gliomas. *Neurol Med Chir (Tokyo)*. 2013;53(7):496–500.
58. Abel R, Jones J, Mandelin P, Cen S, Pagnini P. Distinguishing Pseudoprogression From True Progression by FLAIR Volumetric Characteristics Compared to 45 Gy Isodose Volumes in Treated Glioblastoma Patients. *Int J Radiat Oncol • Biol • Phys*. 2012 Nov 1;84(3):S275.
59. Abdulla S, Saada J, Johnson G, Jefferies S, Ajithkumar T. Tumour progression or pseudoprogression? A review of post-treatment radiological appearances of glioblastoma. *Clin Radiol*. 2015 Nov;70(11):1299–312.
60. Oberheim Bush NA, Cha S, Chang SM, Clarke JL. Chapter 55 - Pseudoprogression in Neuro-Oncology: Overview, Pathophysiology, and Interpretation. In: Newton HB, editor. *Handbook of Neuro-Oncology Neuroimaging (Second Edition)* [Internet]. San Diego: Academic Press; 2016 [cited 2019 Jun 13]. p. 681–95. Available from: <http://www.sciencedirect.com/science/article/pii/B9780128009451000550>
61. Gerstner ER, McNamara MB, Norden AD, LaFrankie D, Wen PY. Effect of adding temozolomide to radiation therapy on the incidence of pseudo-progression. *J Neurooncol*. 2009 Aug;94(1):97–101.
62. Zhang J, Yu H, Qian X, Liu K, Tan H, Yang T, et al. Pseudo progression identification of glioblastoma with dictionary learning. *Comput Biol Med*. 2016 01;73:94–101.
63. Verma R, Zacharaki EI, Ou Y, Cai H, Chawla S, Lee S-K, et al. Multiparametric tissue characterization of brain neoplasms and their recurrence using pattern classification of MR images. *Acad Radiol*. 2008 Aug;15(8):966–77.
64. Asao C, Korogi Y, Kitajima M, Hirai T, Baba Y, Makino K, et al. Diffusion-weighted imaging of radiation-induced brain injury for differentiation from tumor recurrence. *AJNR Am J Neuroradiol*. 2005 Jul;26(6):1455–60.
65. Lee WJ, Choi SH, Park C-K, Yi KS, Kim TM, Lee S-H, et al. Diffusion-weighted MR imaging for the differentiation of true progression from pseudoprogression following

- concomitant radiotherapy with temozolomide in patients with newly diagnosed high-grade gliomas. *Acad Radiol*. 2012 Nov;19(11):1353–61.
66. Xu J-L, Li Y-L, Lian J-M, Dou S, Yan F-S, Wu H, et al. Distinction between postoperative recurrent glioma and radiation injury using MR diffusion tensor imaging. *Neuroradiology*. 2010 Dec;52(12):1193–9.
 67. Hein PA, Eskey CJ, Dunn JF, Hug EB. Diffusion-weighted imaging in the follow-up of treated high-grade gliomas: tumor recurrence versus radiation injury. *AJNR Am J Neuroradiol*. 2004 Feb;25(2):201–9.
 68. Sundgren PC, Fan X, Weybright P, Welsh RC, Carlos RC, Petrou M, et al. Differentiation of recurrent brain tumor versus radiation injury using diffusion tensor imaging in patients with new contrast-enhancing lesions. *Magn Reson Imaging*. 2006 Nov;24(9):1131–42.
 69. Chenevert TL, Stegman LD, Taylor JM, Robertson PL, Greenberg HS, Rehemtulla A, et al. Diffusion magnetic resonance imaging: an early surrogate marker of therapeutic efficacy in brain tumors. *J Natl Cancer Inst*. 2000 Dec 20;92(24):2029–36.
 70. Huang RY, Neagu MR, Reardon DA, Wen PY. Pitfalls in the neuroimaging of glioblastoma in the era of antiangiogenic and immuno/targeted therapy - detecting illusive disease, defining response. *Front Neurol*. 2015;6:33.
 71. Yamasaki F, Kurisu K, Satoh K, Arita K, Sugiyama K, Ohtaki M, et al. Apparent diffusion coefficient of human brain tumors at MR imaging. *Radiology*. 2005 Jun;235(3):985–91.
 72. Sugahara T, Korogi Y, Kochi M, Ikushima I, Shigematu Y, Hirai T, et al. Usefulness of diffusion-weighted MRI with echo-planar technique in the evaluation of cellularity in gliomas. *J Magn Reson Imaging JMRI*. 1999 Jan;9(1):53–60.
 73. Reimer C, Deike K, Graf M, Reimer P, Wiestler B, Floca RO, et al. Differentiation of pseudoprogression and real progression in glioblastoma using ADC parametric response maps. *PLoS ONE [Internet]*. 2017 Apr 6 [cited 2019 Apr 28];12(4). Available from: <https://www.ncbi.nlm.nih.gov/pmc/articles/PMC5383222/>
 74. Zeng Q-S, Li C-F, Liu H, Zhen J-H, Feng D-C. Distinction between recurrent glioma and radiation injury using magnetic resonance spectroscopy in combination with diffusion-weighted imaging. *Int J Radiat Oncol Biol Phys*. 2007 May 1;68(1):151–8.
 75. Jena A, Taneja S, Jha A, Damesha NK, Negi P, Jadhav GK, et al. Multiparametric Evaluation in Differentiating Glioma Recurrence from Treatment-Induced Necrosis Using Simultaneous 18F-FDG-PET/MRI: A Single-Institution Retrospective Study. *AJNR Am J Neuroradiol*. 2017 May;38(5):899–907.
 76. Fink JR, Carr RB, Matsusue E, Iyer RS, Rockhill JK, Haynor DR, et al. Comparison of 3 Tesla proton MR spectroscopy, MR perfusion and MR diffusion for distinguishing glioma recurrence from posttreatment effects. *J Magn Reson Imaging JMRI*. 2012 Jan;35(1):56–63.
 77. Prager AJ, Martinez N, Beal K, Omuro A, Zhang Z, Young RJ. Diffusion and perfusion MRI to differentiate treatment-related changes including pseudoprogression from recurrent tumors in high-grade gliomas with histopathologic evidence. *AJNR Am J Neuroradiol*. 2015 May;36(5):877–85.
 78. Alexiou GA, Zikou A, Tsiouris S, Goussia A, Kosta P, Papadopoulos A, et al. Comparison of diffusion tensor, dynamic susceptibility contrast MRI and (99m)Tc-Tetrofosmin brain SPECT for the detection of recurrent high-grade glioma. *Magn Reson Imaging*. 2014 Sep;32(7):854–9.
 79. Bulik M, Kazda T, Slampa P, Jancalek R. The Diagnostic Ability of Follow-Up Imaging Biomarkers after Treatment of Glioblastoma in the Temozolomide Era: Implications from Proton MR Spectroscopy and Apparent Diffusion Coefficient Mapping [Internet].

BioMed Research International. 2015 [cited 2019 Apr 28]. Available from: <https://www.hindawi.com/journals/bmri/2015/641023/>

80. Kazda T, Bulik M, Pospisil P, Lakomy R, Smrcka M, Slampa P, et al. Advanced MRI increases the diagnostic accuracy of recurrent glioblastoma: Single institution thresholds and validation of MR spectroscopy and diffusion weighted MR imaging. *NeuroImage Clin.* 2016;11:316–21.
81. Bobek-Billewicz B, Stasik-Pres G, Majchrzak H, Zarudzki L. Differentiation between brain tumor recurrence and radiation injury using perfusion, diffusion-weighted imaging and MR spectroscopy. *Folia Neuropathol.* 2010;48(2):81–92.
82. Al Sayyari A, Buckley R, McHenry C, Pannek K, Coulthard A, Rose S. Distinguishing recurrent primary brain tumor from radiation injury: a preliminary study using a susceptibility-weighted MR imaging-guided apparent diffusion coefficient analysis strategy. *AJNR Am J Neuroradiol.* 2010 Jun;31(6):1049–54.
83. Song YS, Choi SH, Park C-K, Yi KS, Lee WJ, Yun TJ, et al. True progression versus pseudoprogression in the treatment of glioblastomas: a comparison study of normalized cerebral blood volume and apparent diffusion coefficient by histogram analysis. *Korean J Radiol.* 2013 Aug;14(4):662–72.
84. Chu HH, Choi SH, Ryoo I, Kim SC, Yeom JA, Shin H, et al. Differentiation of true progression from pseudoprogression in glioblastoma treated with radiation therapy and concomitant temozolomide: comparison study of standard and high-b-value diffusion-weighted imaging. *Radiology.* 2013 Dec;269(3):831–40.
85. Wang S, Martinez-Lage M, Sakai Y, Chawla S, Kim SG, Alonso-Basanta M, et al. Differentiating Tumor Progression from Pseudoprogression in Patients with Glioblastomas Using Diffusion Tensor Imaging and Dynamic Susceptibility Contrast MRI. *AJNR Am J Neuroradiol.* 2016 Jan;37(1):28–36.
86. Thust SC, Heiland S, Falini A, Jäger HR, Waldman AD, Sundgren PC, et al. Glioma imaging in Europe: A survey of 220 centres and recommendations for best clinical practice. *Eur Radiol.* 2018 Aug;28(8):3306–17.
87. Fatterpekar GM, Galheigo D, Narayana A, Johnson G, Knopp E. Treatment-related change versus tumor recurrence in high-grade gliomas: a diagnostic conundrum--use of dynamic susceptibility contrast-enhanced (DSC) perfusion MRI. *AJR Am J Roentgenol.* 2012 Jan;198(1):19–26.
88. Cha J, Kim ST, Kim H-J, Kim B-J, Kim YK, Lee JY, et al. Differentiation of tumor progression from pseudoprogression in patients with posttreatment glioblastoma using multiparametric histogram analysis. *AJNR Am J Neuroradiol.* 2014 Jul;35(7):1309–17.
89. Cha S, Knopp EA, Johnson G, Wetzel SG, Litt AW, Zagzag D. Intracranial mass lesions: dynamic contrast-enhanced susceptibility-weighted echo-planar perfusion MR imaging. *Radiology.* 2002 Apr;223(1):11–29.
90. Patel P, Baradaran H, Delgado D, Askin G, Christos P, John Tsiouris A, et al. MR perfusion-weighted imaging in the evaluation of high-grade gliomas after treatment: a systematic review and meta-analysis. *Neuro-Oncol.* 2017;19(1):118–27.
91. Barajas RF, Chang JS, Segal MR, Parsa AT, McDermott MW, Berger MS, et al. Differentiation of recurrent glioblastoma multiforme from radiation necrosis after external beam radiation therapy with dynamic susceptibility-weighted contrast-enhanced perfusion MR imaging. *Radiology.* 2009 Nov;253(2):486–96.
92. Seeger A, Braun C, Skardelly M, Paulsen F, Schittenhelm J, Ernemann U, et al. Comparison of three different MR perfusion techniques and MR spectroscopy for multiparametric assessment in distinguishing recurrent high-grade gliomas from stable disease. *Acad Radiol.* 2013 Dec;20(12):1557–65.
93. D'Souza MM, Sharma R, Jaimini A, Panwar P, Saw S, Kaur P, et al. 11C-MET

- PET/CT and advanced MRI in the evaluation of tumor recurrence in high-grade gliomas. *Clin Nucl Med*. 2014 Sep;39(9):791–8.
94. Heidemans-Hazelaar C, Verbeek AY, Oosterkamp HM, Van der Kallen B, Vecht CJ. Use of perfusion MR imaging for differentiation between tumor progression and pseudo-progression in recurrent glioblastoma multiforme. *J Clin Oncol*. 2010 May 20;28(15_suppl):2026–2026.
95. Hu LS, Baxter LC, Smith KA, Feuerstein BG, Karis JP, Eschbacher JM, et al. Relative cerebral blood volume values to differentiate high-grade glioma recurrence from posttreatment radiation effect: direct correlation between image-guided tissue histopathology and localized dynamic susceptibility-weighted contrast-enhanced perfusion MR imaging measurements. *AJNR Am J Neuroradiol*. 2009 Mar;30(3):552–8.
96. Hu LS, Eschbacher JM, Heiserman JE, Dueck AC, Shapiro WR, Liu S, et al. Reevaluating the imaging definition of tumor progression: perfusion MRI quantifies recurrent glioblastoma tumor fraction, pseudoprogression, and radiation necrosis to predict survival. *Neuro-Oncol*. 2012 Jul;14(7):919–30.
97. Gasparetto EL, Pawlak MA, Patel SH, Huse J, Woo JH, Krejza J, et al. Posttreatment recurrence of malignant brain neoplasm: accuracy of relative cerebral blood volume fraction in discriminating low from high malignant histologic volume fraction. *Radiology*. 2009 Mar;250(3):887–96.
98. Gahramanov S, Raslan AM, Muldoon LL, Hamilton BE, Rooney WD, Varallyay CG, et al. Potential for differentiation of pseudoprogression from true tumor progression with dynamic susceptibility-weighted contrast-enhanced magnetic resonance imaging using ferumoxytol vs. gadoteridol: a pilot study. *Int J Radiat Oncol Biol Phys*. 2011 Feb 1;79(2):514–23.
99. Kim YH, Oh SW, Lim YJ, Park C-K, Lee S-H, Kang KW, et al. Differentiating radiation necrosis from tumor recurrence in high-grade gliomas: assessing the efficacy of 18F-FDG PET, 11C-methionine PET and perfusion MRI. *Clin Neurol Neurosurg*. 2010 Nov;112(9):758–65.
100. Young RJ, Gupta A, Shah AD, Graber JJ, Chan TA, Zhang Z, et al. MRI perfusion in determining pseudoprogression in patients with glioblastoma. *Clin Imaging*. 2013 Feb;37(1):41–9.
101. Hu X, Wong KK, Young GS, Guo L, Wong ST. Support vector machine multiparametric MRI identification of pseudoprogression from tumor recurrence in patients with resected glioblastoma. *J Magn Reson Imaging JMRI*. 2011 Feb;33(2):296–305.
102. Jain R, Scarpace L, Ellika S, Schultz LR, Rock JP, Rosenblum ML, et al. First-pass perfusion computed tomography: initial experience in differentiating recurrent brain tumors from radiation effects and radiation necrosis. *Neurosurgery*. 2007 Oct;61(4):778–86; discussion 786-787.
103. Boxerman JL, Ellingson BM, Jeyapalan S, Elinzano H, Harris RJ, Rogg JM, et al. Longitudinal DSC-MRI for Distinguishing Tumor Recurrence From Pseudoprogression in Patients With a High-grade Glioma. *Am J Clin Oncol*. 2017 Jun;40(3):228–34.
104. Tsien C, Galbán CJ, Chenevert TL, Johnson TD, Hamstra DA, Sundgren PC, et al. Parametric response map as an imaging biomarker to distinguish progression from pseudoprogression in high-grade glioma. *J Clin Oncol Off J Am Soc Clin Oncol*. 2010 May 1;28(13):2293–9.
105. Shin KE, Ahn KJ, Choi HS, Jung SL, Kim BS, Jeon SS, et al. DCE and DSC MR perfusion imaging in the differentiation of recurrent tumour from treatment-related changes in patients with glioma. *Clin Radiol*. 2014 Jun;69(6):e264-272.
106. Mangla R, Singh G, Ziegelitz D, Milano MT, Korones DN, Zhong J, et al. Changes in relative cerebral blood volume 1 month after radiation-temozolomide therapy can help predict

- overall survival in patients with glioblastoma. *Radiology*. 2010 Aug;256(2):575–84.
107. Kong D-S, Kim ST, Kim E-H, Lim DH, Kim WS, Suh Y-L, et al. Diagnostic dilemma of pseudoprogression in the treatment of newly diagnosed glioblastomas: the role of assessing relative cerebral blood flow volume and oxygen-6-methylguanine-DNA methyltransferase promoter methylation status. *AJNR Am J Neuroradiol*. 2011 Feb;32(2):382–7.
108. Baek HJ, Kim HS, Kim N, Choi YJ, Kim YJ. Percent Change of Perfusion Skewness and Kurtosis: A Potential Imaging Biomarker for Early Treatment Response in Patients with Newly Diagnosed Glioblastomas. *Radiology*. 2012 Sep 1;264(3):834–43.
109. Suh CH, Kim HS, Choi YJ, Kim N, Kim SJ. Prediction of pseudoprogression in patients with glioblastomas using the initial and final area under the curves ratio derived from dynamic contrast-enhanced T1-weighted perfusion MR imaging. *AJNR Am J Neuroradiol*. 2013 Dec;34(12):2278–86.
110. Bisdas S, Naegele T, Ritz R, Dimostheni A, Pfannenbergr C, Reimold M, et al. Distinguishing recurrent high-grade gliomas from radiation injury: a pilot study using dynamic contrast-enhanced MR imaging. *Acad Radiol*. 2011 May;18(5):575–83.
111. Yun TJ, Park C-K, Kim TM, Lee S-H, Kim J-H, Sohn C-H, et al. Glioblastoma treated with concurrent radiation therapy and temozolomide chemotherapy: differentiation of true progression from pseudoprogression with quantitative dynamic contrast-enhanced MR imaging. *Radiology*. 2015 Mar;274(3):830–40.
112. Thomas AA, Arevalo-Perez J, Kaley T, Lyo J, Peck KK, Shi W, et al. Dynamic contrast enhanced T1 MRI perfusion differentiates pseudoprogression from recurrent glioblastoma. *J Neurooncol*. 2015 Oct;125(1):183–90.
113. Choi YJ, Kim HS, Jahng G-H, Kim SJ, Suh DC. Pseudoprogression in patients with glioblastoma: added value of arterial spin labeling to dynamic susceptibility contrast perfusion MR imaging. *Acta Radiol Stockh Swed 1987*. 2013 May;54(4):448–54.
114. Yoo R-E, Choi SH. Recent Application of Advanced MR Imaging to Predict Pseudoprogression in High-grade Glioma Patients. *Magn Reson Med Sci MRMS Off J Jpn Soc Magn Reson Med*. 2016;15(2):165–77.
115. Jovanovic M, Radenkovic S, Stosic-Opincal T, Lavrnica S, Gavrilovic S, Lazovic-Popovic B, et al. Differentiation between progression and pseudoprogression by arterial spin labeling MRI in patients with glioblastoma multiforme. *J BUON Off J Balk Union Oncol*. 2017 Aug;22(4):1061–7.
116. Ozsunar Y, Mullins ME, Kwong K, Hochberg FH, Ament C, Schaefer PW, et al. Glioma recurrence versus radiation necrosis? A pilot comparison of arterial spin-labeled, dynamic susceptibility contrast enhanced MRI, and FDG-PET imaging. *Acad Radiol*. 2010 Mar;17(3):282–90.
117. Lewis R, Bhandari A, McKintosh E, Plowman P, Lansley J, Evanson J, et al. Differentiating tumour progression from pseudoprogression in patients with glioblastoma using multiparametric MRI imaging: Data from Barts Health NHS trust London. *Eur J Surg Oncol*. 2016 Nov 1;42(11):S248–9.
118. Park JE, Kim HS, Goh MJ, Kim SJ, Kim JH. Pseudoprogression in Patients with Glioblastoma: Assessment by Using Volume-weighted Voxel-based Multiparametric Clustering of MR Imaging Data in an Independent Test Set. *Radiology*. 2015 Jun;275(3):792–802.
119. Yoon RG, Kim HS, Paik W, Shim WH, Kim SJ, Kim JH. Different diagnostic values of imaging parameters to predict pseudoprogression in glioblastoma subgroups stratified by MGMT promoter methylation. *Eur Radiol*. 2017 Jan;27(1):255–66.
120. Varallyay CG, Muldoon LL, Gahramanov S, Wu YJ, Goodman JA, Li X, et al. Dynamic MRI using iron oxide nanoparticles to assess early vascular effects of antiangiogenic versus corticosteroid treatment in a glioma model. *J Cereb Blood Flow Metab*

- Off J Int Soc Cereb Blood Flow Metab. 2009 Apr;29(4):853–60.
121. Gahramanov S, Muldoon LL, Varallyay CG, Li X, Kraemer DF, Fu R, et al. Pseudoprogression of glioblastoma after chemo- and radiation therapy: diagnosis by using dynamic susceptibility-weighted contrast-enhanced perfusion MR imaging with ferumoxytol versus gadoteridol and correlation with survival. *Radiology*. 2013 Mar;266(3):842–52.
 122. Barajas RF, Hamilton BE, Schwartz D, McConnell HL, Pettersson DR, Horvath A, et al. Combined iron oxide nanoparticle ferumoxytol and gadolinium contrast enhanced MRI define glioblastoma pseudoprogression. *Neuro-Oncol*. 2019 Mar 18;21(4):517–26.
 123. Ma B, Blakeley JO, Hong X, Zhang H, Jiang S, Blair L, et al. Applying amide proton transfer-weighted MRI to distinguish pseudoprogression from true progression in malignant gliomas. *J Magn Reson Imaging JMRI*. 2016;44(2):456–62.
 124. Zhang H, Ma L, Wang Q, Zheng X, Wu C, Xu B-N. Role of magnetic resonance spectroscopy for the differentiation of recurrent glioma from radiation necrosis: a systematic review and meta-analysis. *Eur J Radiol*. 2014 Dec;83(12):2181–9.
 125. Kamada K, Houkin K, Abe H, Sawamura Y, Kashiwaba T. Differentiation of cerebral radiation necrosis from tumor recurrence by proton magnetic resonance spectroscopy. *Neurol Med Chir (Tokyo)*. 1997 Mar;37(3):250–6.
 126. Rabinov JD, Lee PL, Barker FG, Louis DN, Harsh GR, Cosgrove GR, et al. In vivo 3-T MR spectroscopy in the distinction of recurrent glioma versus radiation effects: initial experience. *Radiology*. 2002 Dec;225(3):871–9.
 127. Anbarloui MR, Ghodsi SM, Khoshnevisan A, Khadivi M, Abdollahzadeh S, Aoude A, et al. Accuracy of magnetic resonance spectroscopy in distinction between radiation necrosis and recurrence of brain tumors. *Iran J Neurol*. 2015 Jan 5;14(1):29–34.
 128. Smith EA, Carlos RC, Junck LR, Tsien CI, Elias A, Sundgren PC. Developing a clinical decision model: MR spectroscopy to differentiate between recurrent tumor and radiation change in patients with new contrast-enhancing lesions. *AJR Am J Roentgenol*. 2009 Feb;192(2):W45-52.
 129. Weybright P, Sundgren PC, Maly P, Hassan DG, Nan B, Rohrer S, et al. Differentiation between brain tumor recurrence and radiation injury using MR spectroscopy. *AJR Am J Roentgenol*. 2005 Dec;185(6):1471–6.
 130. Nakajima T, Kumabe T, Kanamori M, Saito R, Tashiro M, Watanabe M, et al. Differential diagnosis between radiation necrosis and glioma progression using sequential proton magnetic resonance spectroscopy and methionine positron emission tomography. *Neurol Med Chir (Tokyo)*. 2009 Sep;49(9):394–401.
 131. Plotkin M, Eisenacher J, Bruhn H, Wurm R, Michel R, Stockhammer F, et al. 123I-IMT SPECT and 1H MR-spectroscopy at 3.0 T in the differential diagnosis of recurrent or residual gliomas: a comparative study. *J Neurooncol*. 2004 Oct;70(1):49–58.
 132. Elias AE, Carlos RC, Smith EA, Frechtling D, George B, Maly P, et al. MR spectroscopy using normalized and non-normalized metabolite ratios for differentiating recurrent brain tumor from radiation injury. *Acad Radiol*. 2011 Sep;18(9):1101–8.
 133. Di Costanzo A, Scarabino T, Trojsi F, Papolizio T, Bonavita S, de Cristofaro M, et al. Recurrent glioblastoma multiforme versus radiation injury: a multiparametric 3-T MR approach. *Radiol Med (Torino)*. 2014 Aug;119(8):616–24.
 134. Matsusue E, Fink JR, Rockhill JK, Ogawa T, Maravilla KR. Distinction between glioma progression and post-radiation change by combined physiologic MR imaging. *Neuroradiology*. 2010 Apr;52(4):297–306.
 135. Prat R, Galeano I, Lucas A, Martínez JC, Martín M, Amador R, et al. Relative value of magnetic resonance spectroscopy, magnetic resonance perfusion, and 2-(18F) fluoro-2-deoxy-D-glucose positron emission tomography for detection of recurrence or grade increase in gliomas. *J Clin Neurosci Off J Neurosurg Soc Australas*. 2010 Jan;17(1):50–3.

136. Verma G, Chawla S, Mohan S, Wang S, Nasrallah M, Sheriff S, et al. Three-dimensional echo planar spectroscopic imaging for differentiation of true progression from pseudoprogression in patients with glioblastoma. *NMR Biomed*. 2019;32(2):e4042.
137. Kruser TJ, Mehta MP, Robins HI. Pseudoprogression after glioma therapy: a comprehensive review. *Expert Rev Neurother*. 2013 Apr;13(4):389–403.
138. Law I, Albert NL, Arbizu J, Boellaard R, Drzezga A, Galldiks N, et al. Joint EANM/EANO/RANO practice guidelines/SNMMI procedure standards for imaging of gliomas using PET with radiolabelled amino acids and [18F]FDG: version 1.0. *Eur J Nucl Med Mol Imaging*. 2019;46(3):540–57.
139. de Zwart PL, van Dijken BRJ, Holtman GA, Stormezand GN, Dierckx RAJO, Jan van Laar P, et al. Diagnostic Accuracy of PET Tracers for the Differentiation of Tumor Progression from Treatment-Related Changes in High-Grade Glioma: A Systematic Review and Metaanalysis. *J Nucl Med Off Publ Soc Nucl Med*. 2020;61(4):498–504.
140. Galldiks N, Lohmann P, Albert NL, Tonn JC, Langen K-J. Current status of PET imaging in neuro-oncology. *Neuro-Oncol Adv*. 2019 Dec;1(1):vdz010.
141. Nandu H, Wen PY, Huang RY. Imaging in neuro-oncology. *Ther Adv Neurol Disord* [Internet]. 2018 Feb 28 [cited 2020 Nov 29];11. Available from: <https://www.ncbi.nlm.nih.gov/pmc/articles/PMC5833173/>
142. Kertels O, Mihovilovic MI, Linsenmann T, Kessler AF, Tran-Gia J, Kircher M, et al. Clinical Utility of Different Approaches for Detection of Late Pseudoprogression in Glioblastoma With O-(2-[18F]Fluoroethyl)-L-Tyrosine PET. *Clin Nucl Med*. 2019 Sep;44(9):695–701.
143. Oborski MJ, Laymon CM, Lieberman FS, Mountz JM. Distinguishing Pseudoprogression From Progression in High-Grade Gliomas. *Clin Nucl Med* [Internet]. 2013 May [cited 2018 Sep 5];38(5). Available from: <https://www.ncbi.nlm.nih.gov/pmc/articles/PMC3880250/>
144. Langleben DD, Segall GM. PET in differentiation of recurrent brain tumor from radiation injury. *J Nucl Med Off Publ Soc Nucl Med*. 2000 Nov;41(11):1861–7.
145. Horkey LL, Hsiao EM, Weiss SE, Drappatz J, Gerbaudo VH. Dual phase FDG-PET imaging of brain metastases provides superior assessment of recurrence versus post-treatment necrosis. *J Neurooncol*. 2011 May;103(1):137–46.
146. Harat M, Małkowski B, Makarewicz R. Pre-irradiation tumour volumes defined by MRI and dual time-point FET-PET for the prediction of glioblastoma multiforme recurrence: A prospective study. *Radiother Oncol J Eur Soc Ther Radiol Oncol*. 2016 Aug;120(2):241–7.
147. Matuszak J, Waissi W, Clavier JB, Noël G, Namer IJ. Métastases cérébrales : apport de l'acquisition tardive en TEP/TDM au 18F-FDG pour le diagnostic différentiel entre récurrence tumorale et radionécrose. *Médecine Nucl*. 2016 May 1;40(3):196.
148. Padma MV, Said S, Jacobs M, Hwang DR, Dunigan K, Satter M, et al. Prediction of pathology and survival by FDG PET in gliomas. *J Neurooncol*. 2003 Sep;64(3):227–37.
149. Kubota R, Yamada S, Kubota K, Ishiwata K, Tamahashi N, Ido T. Intratumoral distribution of fluorine-18-fluorodeoxyglucose in vivo: high accumulation in macrophages and granulation tissues studied by microautoradiography. *J Nucl Med Off Publ Soc Nucl Med*. 1992 Nov;33(11):1972–80.
150. Chen W. Clinical applications of PET in brain tumors. *J Nucl Med Off Publ Soc Nucl Med*. 2007 Sep;48(9):1468–81.
151. Ricci PE, Karis JP, Heiserman JE, Fram EK, Bice AN, Drayer BP. Differentiating recurrent tumor from radiation necrosis: time for re-evaluation of positron emission tomography? *AJNR Am J Neuroradiol*. 1998 Mar;19(3):407–13.
152. Chen W, Silverman DHS, Delaloye S, Czernin J, Kamdar N, Pope W, et al. 18F-FDOPA PET imaging of brain tumors: comparison study with 18F-FDG PET and evaluation

- of diagnostic accuracy. *J Nucl Med Off Publ Soc Nucl Med*. 2006 Jun;47(6):904–11.
153. Ledezma CJ, Chen W, Sai V, Freitas B, Cloughesy T, Czernin J, et al. 18F-FDOPA PET/MRI fusion in patients with primary/recurrent gliomas: initial experience. *Eur J Radiol*. 2009 Aug;71(2):242–8.
 154. Fueger BJ, Czernin J, Cloughesy T, Silverman DH, Geist CL, Walter MA, et al. Correlation of 6-18F-fluoro-L-dopa PET uptake with proliferation and tumor grade in newly diagnosed and recurrent gliomas. *J Nucl Med Off Publ Soc Nucl Med*. 2010 Oct;51(10):1532–8.
 155. Herrmann K, Czernin J, Cloughesy T, Lai A, Pomykala KL, Benz MR, et al. Comparison of visual and semiquantitative analysis of 18F-FDOPA-PET/CT for recurrence detection in glioblastoma patients. *Neuro-Oncol*. 2014 Apr;16(4):603–9.
 156. Karunanithi S, Sharma P, Kumar A, Khangembam BC, Bandopadhyaya GP, Kumar R, et al. 18F-FDOPA PET/CT for detection of recurrence in patients with glioma: prospective comparison with 18F-FDG PET/CT. *Eur J Nucl Med Mol Imaging*. 2013 Jul;40(7):1025–35.
 157. Yu J, Zheng J, Xu W, Weng J, Gao L, Tao L, et al. Accuracy of 18F-FDOPA Positron Emission Tomography and 18F-FET Positron Emission Tomography for Differentiating Radiation Necrosis from Brain Tumor Recurrence. *World Neurosurg*. 2018 Jun 1;114:e1211–24.
 158. Galldiks N, Dunkl V, Stoffels G, Hutterer M, Rapp M, Sabel M, et al. Diagnosis of pseudoprogression in patients with glioblastoma using O-(2-[18F]fluoroethyl)-L-tyrosine PET. *Eur J Nucl Med Mol Imaging*. 2015 Apr;42(5):685–95.
 159. Galldiks N, Stoffels G, Filss C, Rapp M, Blau T, Tscherpel C, et al. The use of dynamic O-(2-18F-fluoroethyl)-l-tyrosine PET in the diagnosis of patients with progressive and recurrent glioma. *Neuro-Oncol*. 2015 Sep;17(9):1293–300.
 160. Pauleit D, Floeth F, Hamacher K, Riemenschneider MJ, Reifenberger G, Müller H-W, et al. O-(2-[18F]fluoroethyl)-L-tyrosine PET combined with MRI improves the diagnostic assessment of cerebral gliomas. *Brain J Neurol*. 2005 Mar;128(Pt 3):678–87.
 161. Kebir S, Fimmers R, Galldiks N, Schäfer N, Mack F, Schaub C, et al. Late Pseudoprogression in Glioblastoma: Diagnostic Value of Dynamic O-(2-[18F]fluoroethyl)-L-Tyrosine PET. *Clin Cancer Res Off J Am Assoc Cancer Res*. 2016 01;22(9):2190–6.
 162. Mihovilovic MI, Kertels O, Hänscheid H, Löhr M, Monoranu C-M, Kleinlein I, et al. O-(2-(18F)fluoroethyl)-L-tyrosine PET for the differentiation of tumour recurrence from late pseudoprogression in glioblastoma. *J Neurol Neurosurg Psychiatry*. 2019 Feb;90(2):238–9.
 163. Pöpperl G, Götz C, Rachinger W, Gildehaus F-J, Tonn J-C, Tatsch K. Value of O-(2-[18F]fluoroethyl)-L-tyrosine PET for the diagnosis of recurrent glioma. *Eur J Nucl Med Mol Imaging*. 2004 Nov;31(11):1464–70.
 164. Mehrkens JH, Pöpperl G, Rachinger W, Herms J, Seelos K, Tatsch K, et al. The positive predictive value of O-(2-[18F]fluoroethyl)-L-tyrosine (FET) PET in the diagnosis of a glioma recurrence after multimodal treatment. *J Neurooncol*. 2008 May;88(1):27–35.
 165. Kebir S, Khurshid Z, Gaertner FC, Essler M, Hattingen E, Fimmers R, et al. Unsupervised consensus cluster analysis of [18F]-fluoroethyl-L-tyrosine positron emission tomography identified textural features for the diagnosis of pseudoprogression in high-grade glioma. *Oncotarget*. 2017 Jan 31;8(5):8294–304.
 166. Rachinger W, Goetz C, Pöpperl G, Gildehaus FJ, Kreth FW, Holtmannspötter M, et al. Positron emission tomography with O-(2-[18F]fluoroethyl)-l-tyrosine versus magnetic resonance imaging in the diagnosis of recurrent gliomas. *Neurosurgery*. 2005 Sep;57(3):505–11; discussion 505-511.
 167. Werner J-M, Stoffels G, Lichtenstein T, Borggreffe J, Lohmann P, Ceccon G, et al. Differentiation of treatment-related changes from tumour progression: a direct comparison between dynamic FET PET and ADC values obtained from DWI MRI. *Eur J Nucl Med Mol*

Imaging. 2019 Aug;46(9):1889–901.

168. Grosu A-L, Astner ST, Riedel E, Nieder C, Wiedenmann N, Heinemann F, et al. An interindividual comparison of O-(2-[18F]fluoroethyl)-L-tyrosine (FET)- and L-[methyl-11C]methionine (MET)-PET in patients with brain gliomas and metastases. *Int J Radiat Oncol Biol Phys*. 2011 Nov 15;81(4):1049–58.

169. Tsuyuguchi N, Takami T, Sunada I, Iwai Y, Yamanaka K, Tanaka K, et al. Methionine positron emission tomography for differentiation of recurrent brain tumor and radiation necrosis after stereotactic radiosurgery--in malignant glioma. *Ann Nucl Med*. 2004 Jun;18(4):291–6.

170. De Witte O, Goldberg I, Wikler D, Rorive S, Damhaut P, Monclus M, et al. Positron emission tomography with injection of methionine as a prognostic factor in glioma. *J Neurosurg*. 2001 Nov;95(5):746–50.

171. Matsuo M, Miwa K, Shinoda J, Tanaka O, Krishna M. Impact of C11-methionine Positron Emission Tomography (PET) for Malignant Glioma in Radiation Therapy: Is C11-methionine PET a superior to Magnetic Resonance Imaging? *Int J Radiat Oncol • Biol • Phys*. 2011 Oct 1;81(2):S182.

172. Matsuo M, Tanaka H, Yamaguchi T, Nishibori H, Ogawa S. Pseudoprogression of Glioblastoma Multiforme After Chemoradiation Therapy: Diagnosis by 11C-Methionine Positron Emission Tomography (PET). *Int J Radiat Oncol • Biol • Phys*. 2016 Oct 1;96(2):E102.

173. Tripathi M, Sharma R, Varshney R, Jaimini A, Jain J, Souza MMD, et al. Comparison of F-18 FDG and C-11 methionine PET/CT for the evaluation of recurrent primary brain tumors. *Clin Nucl Med*. 2012 Feb;37(2):158–63.

174. Terakawa Y, Tsuyuguchi N, Iwai Y, Yamanaka K, Higashiyama S, Takami T, et al. Diagnostic accuracy of 11C-methionine PET for differentiation of recurrent brain tumors from radiation necrosis after radiotherapy. *J Nucl Med Off Publ Soc Nucl Med*. 2008 May;49(5):694–9.

175. Garcia JR, Cozar M, Baquero M, Fernández Barrionuevo JM, Jaramillo A, Rubio J, et al. The value of 11C-methionine PET in the early differentiation between tumour recurrence and radionecrosis in patients treated for a high-grade glioma and indeterminate MRI. *Rev Espanola Med Nucl E Imagen Mol*. 2017 Apr;36(2):85–90.

176. Minamimoto R, Saginoya T, Kondo C, Tomura N, Ito K, Matsuo Y, et al. Differentiation of Brain Tumor Recurrence from Post-Radiotherapy Necrosis with 11C-Methionine PET: Visual Assessment versus Quantitative Assessment. *PLoS One*. 2015;10(7):e0132515.

177. Li D-L, Xu Y-K, Wang Q-S, Wu H-B, Li H-S. ¹¹C-methionine and ¹⁸F-fluorodeoxyglucose positron emission tomography/CT in the evaluation of patients with suspected primary and residual/recurrent gliomas. *Chin Med J (Engl)*. 2012 Jan;125(1):91–6.

178. Van Laere K, Ceysens S, Van Calenbergh F, de Groot T, Menten J, Flamen P, et al. Direct comparison of 18F-FDG and 11C-methionine PET in suspected recurrence of glioma: sensitivity, inter-observer variability and prognostic value. *Eur J Nucl Med Mol Imaging*. 2005 Jan;32(1):39–51.

179. Dandois V, Rommel D, Renard L, Jamart J, Cosnard G. Substitution of 11C-methionine PET by perfusion MRI during the follow-up of treated high-grade gliomas: preliminary results in clinical practice. *J Neuroradiol J Neuroradiol*. 2010 May;37(2):89–97.

180. Deuschl C, Kirchner J, Poeppel TD, Schaarschmidt B, Kebir S, El Hindy N, et al. 11C-MET PET/MRI for detection of recurrent glioma. *Eur J Nucl Med Mol Imaging*. 2018;45(4):593–601.

181. Collet S, Valable S, Constans JM, Lechapt-Zalcman E, Roussel S, Delcroix N, et al. [18F]-fluoro-l-thymidine PET and advanced MRI for preoperative grading of gliomas.

NeuroImage Clin. 2015 May 29;8:448–54.

182. Chen W, Cloughesy T, Kamdar N, Satyamurthy N, Bergsneider M, Liau L, et al. Imaging proliferation in brain tumors with 18F-FLT PET: comparison with 18F-FDG. *J Nucl Med Off Publ Soc Nucl Med*. 2005 Jun;46(6):945–52.
183. Jacobs AH, Thomas A, Kracht LW, Li H, Dittmar C, Garlip G, et al. 18F-fluoro-L-thymidine and 11C-methylmethionine as markers of increased transport and proliferation in brain tumors. *J Nucl Med Off Publ Soc Nucl Med*. 2005 Dec;46(12):1948–58.
184. Ullrich R, Backes H, Li H, Kracht L, Miletic H, Kesper K, et al. Glioma proliferation as assessed by 3'-fluoro-3'-deoxy-L-thymidine positron emission tomography in patients with newly diagnosed high-grade glioma. *Clin Cancer Res Off J Am Assoc Cancer Res*. 2008 Apr 1;14(7):2049–55.
185. Choi SJ, Kim JS, Kim JH, Oh SJ, Lee JG, Kim CJ, et al. [18F]3'-deoxy-3'-fluorothymidine PET for the diagnosis and grading of brain tumors. *Eur J Nucl Med Mol Imaging*. 2005 Jun;32(6):653–9.
186. Schiepers C, Dahlbom M, Chen W, Cloughesy T, Czernin J, Phelps ME, et al. Kinetics of 3'-deoxy-3'-18F-fluorothymidine during treatment monitoring of recurrent high-grade glioma. *J Nucl Med Off Publ Soc Nucl Med*. 2010 May;51(5):720–7.
187. Wardak M, Schiepers C, Dahlbom M, Cloughesy T, Chen W, Satyamurthy N, et al. Discriminant analysis of ¹⁸F-fluorothymidine kinetic parameters to predict survival in patients with recurrent high-grade glioma. *Clin Cancer Res Off J Am Assoc Cancer Res*. 2011 Oct 15;17(20):6553–62.
188. Dhermain FG, Hau P, Lanfermann H, Jacobs AH, van den Bent MJ. Advanced MRI and PET imaging for assessment of treatment response in patients with gliomas. *Lancet Neurol*. 2010 Sep;9(9):906–20.
189. Muzi M, Spence AM, O'Sullivan F, Mankoff DA, Wells JM, Grierson JR, et al. Kinetic analysis of 3'-deoxy-3'-18F-fluorothymidine in patients with gliomas. *J Nucl Med Off Publ Soc Nucl Med*. 2006 Oct;47(10):1612–21.
190. Spence AM, Muzi M, Link JM, O'Sullivan F, Eary JF, Hoffman JM, et al. NCI-sponsored trial for the evaluation of safety and preliminary efficacy of 3'-deoxy-3'-[18F]fluorothymidine (FLT) as a marker of proliferation in patients with recurrent gliomas: preliminary efficacy studies. *Mol Imaging Biol MIB Off Publ Acad Mol Imaging*. 2009 Oct;11(5):343–55.
191. den Hollander MW, Enting RH, de Groot JC, Solouki MA, den Dunnen WFA, Sluiter WJ, et al. Prospective analysis of serial FLT-PET scanning to discriminate between true and pseudoprogression in glioblastoma. *J Clin Oncol*. 2014 May 20;32(15_suppl):2009–2009.
192. Brahm CG, den Hollander MW, Enting RH, de Groot JC, Solouki AM, den Dunnen WFA, et al. Serial FLT PET imaging to discriminate between true progression and pseudoprogression in patients with newly diagnosed glioblastoma: a long-term follow-up study. *Eur J Nucl Med Mol Imaging*. 2018 Jul 21;
193. Enslow MS, Zollinger LV, Morton KA, Kadmas DJ, Butterfield RI, Christian PE, et al. Comparison of F-18 Fluorodeoxyglucose and F-18 Fluorothymidine Positron Emission Tomography in Differentiating Radiation Necrosis from Recurrent Glioma. *Clin Nucl Med*. 2012 Sep;37(9):854–61.
194. Gulyás B, Halldin C. New PET radiopharmaceuticals beyond FDG for brain tumor imaging. *Q J Nucl Med Mol Imaging Off Publ Ital Assoc Nucl Med AIMN Int Assoc Radiopharmacol IAR Sect Soc Of*. 2012 Apr;56(2):173–90.
195. Alkonyi B, Barger GR, Mittal S, Muzik O, Chugani DC, Bahl G, et al. Accurate differentiation of recurrent gliomas from radiation injury by kinetic analysis of α -11C-methyl-L-tryptophan PET. *J Nucl Med Off Publ Soc Nucl Med*. 2012 Jul;53(7):1058–64.
196. Galldiks N, Law I, Pope WB, Arbizu J, Langen K-J. The use of amino acid PET and

- conventional MRI for monitoring of brain tumor therapy. *NeuroImage Clin.* 2017;13:386–94.
197. Barajas RF, Krohn KA, Link JM, Hawkins RA, Clarke JL, Pampaloni MH, et al. Glioma FMISO PET/MR Imaging Concurrent with Antiangiogenic Therapy: Molecular Imaging as a Clinical Tool in the Burgeoning Era of Personalized Medicine. *Biomedicines.* 2016 Oct 31;4(4).
198. Bolcaen J, Descamps B, Deblaere K, Boterberg T, De Vos Pharm F, Kalala J-P, et al. (18)F-fluoromethylcholine (FCho), (18)F-fluoroethyltyrosine (FET), and (18)F-fluorodeoxyglucose (FDG) for the discrimination between high-grade glioma and radiation necrosis in rats: a PET study. *Nucl Med Biol.* 2015 Jan;42(1):38–45.
199. Beshr R, Isohashi K, Watabe T, Naka S, Horitsugi G, Romanov V, et al. Preliminary feasibility study on differential diagnosis between radiation-induced cerebral necrosis and recurrent brain tumor by means of [18F]fluoro-borono-phenylalanine PET/CT. *Ann Nucl Med.* 2018 Dec;32(10):702–8.
200. Miyashita M, Miyatake S-I, Imahori Y, Yokoyama K, Kawabata S, Kajimoto Y, et al. Evaluation of fluoride-labeled boronophenylalanine-PET imaging for the study of radiation effects in patients with glioblastomas. *J Neurooncol.* 2008 Sep;89(2):239–46.
201. Zhang H, Ma L, Wu C, Xu B. Performance of SPECT in the differential diagnosis of glioma recurrence from radiation necrosis. *J Clin Neurosci Off J Neurosurg Soc Australas.* 2015 Feb;22(2):229–37.
202. Tie J, Gunawardana DH, Rosenthal MA. Differentiation of tumor recurrence from radiation necrosis in high-grade gliomas using 201Tl-SPECT. *J Clin Neurosci Off J Neurosurg Soc Australas.* 2008 Dec;15(12):1327–34.
203. Caresia AP, Castell-Conesa J, Negre M, Mestre A, Cuberas G, Mañes A, et al. Thallium-201SPECT assessment in the detection of recurrences of treated gliomas and ependymomas. *Clin Transl Oncol.* 2006 Oct 1;8(10):750–4.
204. Vos MJ, Tony BN, Hoekstra OS, Postma TJ, Heimans JJ, Hooft L. Systematic review of the diagnostic accuracy of 201Tl single photon emission computed tomography in the detection of recurrent glioma. *Nucl Med Commun.* 2007 Jun;28(6):431–9.
205. Gómez-Río M, Rodríguez-Fernández A, Ramos-Font C, López-Ramírez E, Llamas-Elvira JM. Diagnostic accuracy of 201Thallium-SPECT and 18F-FDG-PET in the clinical assessment of glioma recurrence. *Eur J Nucl Med Mol Imaging.* 2008 May;35(5):966–75.
206. Jeune FP –Le, Dubois F, Blond S, Steinling M. Sestamibi technetium-99m brain single-photon emission computed tomography to identify recurrent glioma in adults: 201 studies. *J Neurooncol.* 2006 Apr 1;77(2):177–83.
207. Palumbo B, Lupattelli M, Pelliccioli GP, Chiarini P, Moschini TO, Palumbo I, et al. Association of 99mTc-MIBI brain SPECT and proton magnetic resonance spectroscopy (1H-MRS) to assess glioma recurrence after radiotherapy. *Q J Nucl Med Mol Imaging Off Publ Ital Assoc Nucl Med AIMN Int Assoc Radiopharmacol IAR Sect Soc Of.* 2006 Mar;50(1):88–93.
208. Amin A, Moustafa H, Ahmed E, El-Toukhy M. Glioma residual or recurrence versus radiation necrosis: accuracy of pentavalent technetium-99m-dimercaptosuccinic acid [Tc-99m (V) DMSA] brain SPECT compared to proton magnetic resonance spectroscopy (1H-MRS): initial results. *J Neurooncol.* 2012 Feb;106(3):579–87.
209. Alexiou GA, Fotopoulos AD, Papadopoulos A, Kyritsis AP, Polyzoidis KS, Tsiouris S. Evaluation of brain tumor recurrence by (99m)Tc-tetrofosmin SPECT: a prospective pilot study. *Ann Nucl Med.* 2007 Jul;21(5):293–8.
210. Arora G, Sharma P, Sharma A, Mishra A, Hazari P, Biswas A, et al. 99mTc-Methionine Hybrid SPECT/CT for Detection of Recurrent Glioma. *Clin Nucl Med [Internet].* 2018 May 1 [cited 2019 May 9];43(5). Available from: insights.ovid.com
211. Santra A, Kumar R, Sharma P. Use of 99m-technetium-glucoheptonate as a tracer for

- brain tumor imaging: An overview of its strengths and pitfalls. *Indian J Nucl Med IJNM Off J Soc Nucl Med India*. 2015;30(1):1–8.
212. Rani N, Singh B, Kumar N, Singh P, Hazari PP, Singh H, et al. Differentiation of Recurrent/Residual Glioma From Radiation Necrosis Using Semi Quantitative ^{99m}Tc MDM (Bis-Methionine-DTPA) Brain SPECT/CT and Dynamic Susceptibility Contrast-Enhanced MR Perfusion: A Comparative Study. *Clin Nucl Med*. 2018 Mar;43(3):e74–81.
213. Van Mieghem E, Wozniak A, Geussens Y, Menten J, De Vleeschouwer S, Van Calenbergh F, et al. Defining pseudoprogression in glioblastoma multiforme. *Eur J Neurol*. 2013 Oct;20(10):1335–41.
214. de Wit MCY, de Bruin HG, Eijkenboom W, Sillevius Smitt P a. E, van den Bent MJ. Immediate post-radiotherapy changes in malignant glioma can mimic tumor progression. *Neurology*. 2004 Aug 10;63(3):535–7.
215. Li H, Li J, Cheng G, Zhang J, Li X. IDH mutation and MGMT promoter methylation are associated with the pseudoprogression and improved prognosis of glioblastoma multiforme patients who have undergone concurrent and adjuvant temozolomide-based chemoradiotherapy. *Clin Neurol Neurosurg*. 2016 Dec;151:31–6.
216. Balaña C, Capellades J, Pineda E, Estival A, Puig J, Domenech S, et al. Pseudoprogression as an adverse event of glioblastoma therapy. *Cancer Med*. 2017 Dec;6(12):2858–66.
217. Soike MH, McTyre ER, Shah N, Puchalski RB, Holmes JA, Paulsson AK, et al. Glioblastoma radiomics: can genomic and molecular characteristics correlate with imaging response patterns? *Neuroradiology*. 2018 Oct;60(10):1043–51.
218. Elshafeey N, Kotrotsou A, Hassan A, Elshafei N, Hassan I, Ahmed S, et al. Multicenter study demonstrates radiomic features derived from magnetic resonance perfusion images identify pseudoprogression in glioblastoma. *Nat Commun*. 2019 Jul 18;10(1):3170.
219. Ismail M, Hill V, Statsevych V, Huang R, Prasanna P, Correa R, et al. Shape Features of the Lesion Habitat to Differentiate Brain Tumor Progression from Pseudoprogression on Routine Multiparametric MRI: A Multisite Study. *AJNR Am J Neuroradiol*. 2018 Dec;39(12):2187–93.
220. Galldiks N, Kocher M, Langen K-J. Pseudoprogression after glioma therapy: an update. *Expert Rev Neurother*. 2017 Nov;17(11):1109–15.
221. Bacchi S, Zerner T, Dongas J, Asahina AT, Abou-Hamden A, Otto S, et al. Deep learning in the detection of high-grade glioma recurrence using multiple MRI sequences: A pilot study. *J Clin Neurosci Off J Neurosurg Soc Australas*. 2019 Dec;70:11–3.
222. Gao Y, Xiao X, Han B, Li G, Ning X, Wang D, et al. Deep Learning Methodology for Differentiating Glioma Recurrence From Radiation Necrosis Using Multimodal Magnetic Resonance Imaging: Algorithm Development and Validation. *JMIR Med Inform*. 2020 Nov 17;8(11):e19805.
223. Bani-Sadr A, Eker OF, Berner L-P, Ameli R, Hermier M, Barritault M, et al. Conventional MRI radiomics in patients with suspected early- or pseudo-progression. *Neuro-Oncol Adv*. 2019 Dec;1(1):vdz019.
224. Clark K, Vendt B, Smith K, Freymann J, Kirby J, Koppel P, et al. The Cancer Imaging Archive (TCIA): Maintaining and Operating a Public Information Repository. *J Digit Imaging*. 2013 Dec;26(6):1045–57.
225. Rudie JD, Rauschecker AM, Bryan RN, Davatzikos C, Mohan S. Emerging Applications of Artificial Intelligence in Neuro-Oncology. *Radiology*. 2019;290(3):607–18.
226. Kebir S, Schmidt T, Weber M, Lazaridis L, Galldiks N, Langen K-J, et al. A Preliminary Study on Machine Learning-Based Evaluation of Static and Dynamic FET-PET for the Detection of Pseudoprogression in Patients with IDH-Wildtype Glioblastoma. *Cancers*. 2020 Oct 22;12(11).

227. Artzi M, Liberman G, Nadav G, Blumenthal DT, Bokstein F, Aizenstein O, et al. Differentiation between treatment-related changes and progressive disease in patients with high grade brain tumors using support vector machine classification based on DCE MRI. *J Neurooncol.* 2016 May;127(3):515–24.
228. Li M, Tang H, Chan MD, Zhou X, Qian X. DC-AL GAN: Pseudoprogression and true tumor progression of glioblastoma multiform image classification based on DCGAN and AlexNet. *Med Phys.* 2020 Mar;47(3):1139–50.
229. Qian X, Tan H, Zhang J, Liu K, Yang T, Wang M, et al. Identification of biomarkers for pseudo and true progression of GBM based on radiogenomics study. *Oncotarget.* 2016 Aug 23;7(34):55377–94.
230. Jang B-S, Jeon SH, Kim IH, Kim IA. Prediction of Pseudoprogression versus Progression using Machine Learning Algorithm in Glioblastoma. *Sci Rep.* 2018 Aug 21;8(1):12516.
231. Lersy F, Boulouis G, Clément O, Desal H, Anxionnat R, Berge J, et al. Consensus Guidelines of the French Society of Neuroradiology (SFNR) on the use of Gadolinium-Based Contrast agents (GBCAs) and related MRI protocols in Neuroradiology. *J Neuroradiol J Neuroradiol.* 2020 Nov;47(6):441–9.
232. Girardi M, Kay J, Elston DM, Leboit PE, Abu-Alfa A, Cowper SE. Nephrogenic systemic fibrosis: clinicopathological definition and workup recommendations. *J Am Acad Dermatol.* 2011 Dec;65(6):1095-1106.e7.
233. Mathur M, Jones JR, Weinreb JC. Gadolinium Deposition and Nephrogenic Systemic Fibrosis: A Radiologist’s Primer. *Radiogr Rev Publ Radiol Soc N Am Inc.* 2020 Feb;40(1):153–62.
234. Errante Y, Cirimele V, Mallio CA, Di Lazzaro V, Zobel BB, Quattrocchi CC. Progressive increase of T1 signal intensity of the dentate nucleus on unenhanced magnetic resonance images is associated with cumulative doses of intravenously administered gadodiamide in patients with normal renal function, suggesting dechelation. *Invest Radiol.* 2014 Oct;49(10):685–90.
235. Le Goff S, Barrat J-A, Chauvaud L, Paulet Y-M, Gueguen B, Ben Salem D. Compound-specific recording of gadolinium pollution in coastal waters by great scallops. *Sci Rep.* 2019 29;9(1):8015.
236. Schmidt K, Bau M, Merschel G, Tepe N. Anthropogenic gadolinium in tap water and in tap water-based beverages from fast-food franchises in six major cities in Germany. *Sci Total Environ.* 2019 Oct 15;687:1401–8.
237. Walker DT, Davenport MS, McGrath TA, McInnes MDF, Shankar T, Schieda N. Breakthrough Hypersensitivity Reactions to Gadolinium-based Contrast Agents and Strategies to Decrease Subsequent Reaction Rates: A Systematic Review and Meta-Analysis. *Radiology.* 2020 Aug;296(2):312–21.
238. Karsy M, Yoon N, Boettcher L, Jensen R, Shah L, MacDonald J, et al. Surgical treatment of glioblastoma in the elderly: the impact of complications. *J Neurooncol.* 2018 May;138(1):123–32.
239. Gulati S, Jakola AS, Nerland US, Weber C, Solheim O. The risk of getting worse: surgically acquired deficits, perioperative complications, and functional outcomes after primary resection of glioblastoma. *World Neurosurg.* 2011 Dec;76(6):572–9.
240. Schwartz C, Romagna A, Stefanits H, Zimmermann G, Ladisich B, Geiger P, et al. Risks and Benefits of Glioblastoma Resection in Older Adults: A Retrospective Austrian Multicenter Study. *World Neurosurg.* 2020 Jan;133:e583–91.
241. Dimou J, Beland B, Kelly J. Supramaximal resection: A systematic review of its safety, efficacy and feasibility in glioblastoma. *J Clin Neurosci Off J Neurosurg Soc Australas.* 2020 Feb;72:328–34.

242. Baron RB, Lakomkin N, Schupper AJ, Nistal D, Nael K, Price G, et al. Postoperative outcomes following glioblastoma resection using a robot-assisted digital surgical exoscope: a case series. *J Neurooncol*. 2020 Jul;148(3):519–27.
243. Laurent D, Freedman R, Cope L, Sacks P, Abbatematteo J, Kubilis P, et al. Impact of Extent of Resection on Incidence of Postoperative Complications in Patients With Glioblastoma. *Neurosurgery*. 2020 01;86(5):625–30.
244. Cebula H, Todeschi J, Le Fèvre C, Antoni D, Ollivier I, Chibbaro S, et al. [What is the place of surgery in the management of brain metastases in 2020?]. *Cancer Radiother J Soc Francaise Radiother Oncol*. 2020 Oct;24(6–7):470–6.
245. Rahmani R, Tomlinson SB, Santangelo G, Warren KT, Schmidt T, Walter KA, et al. Risk factors associated with early adverse outcomes following craniotomy for malignant glioma in older adults. *J Geriatr Oncol*. 2020 May;11(4):694–700.
246. Grossman R, Sadetzki S, Spiegelmann R, Ram Z. Haemorrhagic complications and the incidence of asymptomatic bleeding associated with stereotactic brain biopsies. *Acta Neurochir (Wien)*. 2005 Jun;147(6):627–31; discussion 631.
247. Heper AO, Erden E, Savas A, Ceyhan K, Erden I, Akyar S, et al. An analysis of stereotactic biopsy of brain tumors and nonneoplastic lesions: a prospective clinicopathologic study. *Surg Neurol*. 2005;64 Suppl 2:S82–88.
248. Smith JS, Quiñones-Hinojosa A, Barbaro NM, McDermott MW. Frame-based stereotactic biopsy remains an important diagnostic tool with distinct advantages over frameless stereotactic biopsy. *J Neurooncol*. 2005 Jun;73(2):173–9.
249. Woodworth GF, McGirt MJ, Samdani A, Garonzik I, Olivi A, Weingart JD. Frameless image-guided stereotactic brain biopsy procedure: diagnostic yield, surgical morbidity, and comparison with the frame-based technique. *J Neurosurg*. 2006 Feb;104(2):233–7.
250. Dammers R, Haitsma IK, Schouten JW, Kros JM, Avezaat CJJ, Vincent AJPE. Safety and efficacy of frameless and frame-based intracranial biopsy techniques. *Acta Neurochir (Wien)*. 2008 Jan;150(1):23–9.
251. Kongkham PN, Knifed E, Tamber MS, Bernstein M. Complications in 622 cases of frame-based stereotactic biopsy, a decreasing procedure. *Can J Neurol Sci J Can Sci Neurol*. 2008 Mar;35(1):79–84.
252. Chen C-C, Hsu P-W, Erich Wu T-W, Lee S-T, Chang C-N, Wei K, et al. Stereotactic brain biopsy: Single center retrospective analysis of complications. *Clin Neurol Neurosurg*. 2009 Dec;111(10):835–9.
253. Owen CM, Linskey ME. Frame-based stereotaxy in a frameless era: current capabilities, relative role, and the positive- and negative predictive values of blood through the needle. *J Neurooncol*. 2009 May;93(1):139–49.
254. Bekelis K, Radwan TA, Desai A, Roberts DW. Frameless robotically targeted stereotactic brain biopsy: feasibility, diagnostic yield, and safety. *J Neurosurg*. 2012 May;116(5):1002–6.
255. Lefranc M, Capel C, Pruvot AS, Fichten A, Desenclos C, Toussaint P, et al. The impact of the reference imaging modality, registration method and intraoperative flat-panel computed tomography on the accuracy of the ROSA® stereotactic robot. *Stereotact Funct Neurosurg*. 2014;92(4):242–50.
256. Lu Y, Yeung C, Radmanesh A, Wiemann R, Black PM, Golby AJ. Comparative effectiveness of frame-based, frameless, and intraoperative magnetic resonance imaging-guided brain biopsy techniques. *World Neurosurg*. 2015 Mar;83(3):261–8.
257. Nishihara M, Takeda N, Harada T, Kidoguchi K, Tatsumi S, Tanaka K, et al. Diagnostic yield and morbidity by neuronavigation-guided frameless stereotactic biopsy using magnetic resonance imaging and by frame-based computed tomography-guided stereotactic biopsy. *Surg Neurol Int*. 2014;5(Suppl 8):S421–426.

258. Georgiopoulos M, Ellul J, Chroni E, Constantoyannis C. Efficacy, Safety, and Duration of a Frameless Fiducial-Less Brain Biopsy versus Frame-based Stereotactic Biopsy: A Prospective Randomized Study. *J Neurol Surg Part Cent Eur Neurosurg*. 2018 Jan;79(1):31–8.
259. Yasin H, Hoff H-J, Blümcke I, Simon M. Experience with 102 Frameless Stereotactic Biopsies Using the neuromate Robotic Device. *World Neurosurg*. 2019 Mar;123:e450–6.
260. Mizobuchi Y, Nakajima K, Fujihara T, Matsuzaki K, Mure H, Nagahiro S, et al. The risk of hemorrhage in stereotactic biopsy for brain tumors. *J Med Investig JMI*. 2019;66(3.4):314–8.
261. Gerlinger M, Rowan AJ, Horswell S, Math M, Larkin J, Endesfelder D, et al. Intratumor Heterogeneity and Branched Evolution Revealed by Multiregion Sequencing. *N Engl J Med*. 2012 Mar 8;366(10):883–92.
262. Zachariah MA, Oliveira-Costa JP, Carter BS, Stott SL, Nahed BV. Blood-based biomarkers for the diagnosis and monitoring of gliomas. *Neuro-Oncol*. 2018 Aug 2;20(9):1155–61.
263. Klekner Á, Szivos L, Virga J, Árkosy P, Bognár L, Birkó Z, et al. Significance of liquid biopsy in glioblastoma - A review. *J Biotechnol*. 2019 Jun 10;298:82–7.
264. Yekula A, Muralidharan K, Rosh ZS, Youngkin AE, Kang KM, Balaj L, et al. Liquid Biopsy Strategies to Distinguish Progression from Pseudoprogression and Radiation Necrosis in Glioblastomas. *Adv Biosyst*. 2020 Jun 2;e2000029.
265. Sareen H, Garrett C, Lynch D, Powter B, Brungs D, Cooper A, et al. The Role of Liquid Biopsies in Detecting Molecular Tumor Biomarkers in Brain Cancer Patients. *Cancers*. 2020 Jul 8;12(7).
266. Smith ER, Zurakowski D, Saad A, Scott RM, Moses MA. Urinary biomarkers predict brain tumor presence and response to therapy. *Clin Cancer Res Off J Am Assoc Cancer Res*. 2008 Apr 15;14(8):2378–86.
267. Loo HK, Mathen P, Lee J, Camphausen K. Circulating biomarkers for high-grade glioma. *Biomark Med*. 2019;13(3):161–5.
268. van Schaijik B, Wickremesekera AC, Mantamadiotis T, Kaye AH, Tan ST, Stylli SS, et al. Circulating tumor stem cells and glioblastoma: A review. *J Clin Neurosci Off J Neurosurg Soc Australas*. 2019 Mar;61:5–9.
269. Liu T, Xu H, Huang M, Ma W, Saxena D, Lustig RA, et al. Circulating Glioma Cells Exhibit Stem Cell-like Properties. *Cancer Res*. 2018 Dec 1;78(23):6632–42.
270. Krol I, Castro-Giner F, Maurer M, Gkoutela S, Szczerba BM, Scherrer R, et al. Detection of circulating tumour cell clusters in human glioblastoma. *Br J Cancer*. 2018 Aug;119(4):487–91.
271. Shankar GM, Balaj L, Stott SL, Nahed B, Carter BS. Liquid biopsy for brain tumors. *Expert Rev Mol Diagn*. 2017;17(10):943–7.
272. Silantsev AS, Falzone L, Libra M, Gurina OI, Kardashova KS, Nikolouzakis TK, et al. Current and Future Trends on Diagnosis and Prognosis of Glioblastoma: From Molecular Biology to Proteomics. *Cells*. 2019 09;8(8).
273. Müller Bark J, Kulasinghe A, Chua B, Day BW, Punyadeera C. Circulating biomarkers in patients with glioblastoma. *Br J Cancer*. 2020;122(3):295–305.
274. Bagley SJ, Nabavizadeh SA, Mays JJ, Till JE, Ware JB, Levy S, et al. Clinical Utility of Plasma Cell-Free DNA in Adult Patients with Newly Diagnosed Glioblastoma: A Pilot Prospective Study. *Clin Cancer Res Off J Am Assoc Cancer Res*. 2020 15;26(2):397–407.
275. Raza IJ, Tingate CA, Gkolia P, Romero L, Tee JW, Hunn MK. Blood Biomarkers of Glioma in Response Assessment Including Pseudoprogression and Other Treatment Effects: A Systematic Review. *Front Oncol*. 2020;10:1191.
276. Chistiakov DA, Chekhonin VP. Circulating tumor cells and their advances to promote

- cancer metastasis and relapse, with focus on glioblastoma multiforme. *Exp Mol Pathol*. 2018;105(2):166–74.
277. Piccioni DE, Achrol AS, Kiedrowski LA, Banks KC, Boucher N, Barkhoudarian G, et al. Analysis of cell-free circulating tumor DNA in 419 patients with glioblastoma and other primary brain tumors. *CNS Oncol*. 2019;8(2):CNS34.
278. Figueroa JM, Carter BS. Detection of glioblastoma in biofluids. *J Neurosurg*. 2018;129(2):334–40.
279. Sullivan JP, Nahed BV, Madden MW, Oliveira SM, Springer S, Bhere D, et al. Brain tumor cells in circulation are enriched for mesenchymal gene expression. *Cancer Discov*. 2014 Nov;4(11):1299–309.
280. Haber DA, Velculescu VE. Blood-based analyses of cancer: circulating tumor cells and circulating tumor DNA. *Cancer Discov*. 2014 Jun;4(6):650–61.
281. Macarthur KM, Kao GD, Chandrasekaran S, Alonso-Basanta M, Chapman C, Lustig RA, et al. Detection of brain tumor cells in the peripheral blood by a telomerase promoter-based assay. *Cancer Res*. 2014 Apr 15;74(8):2152–9.
282. Müller C, Holtschmidt J, Auer M, Heitzer E, Lamszus K, Schulte A, et al. Hematogenous dissemination of glioblastoma multiforme. *Sci Transl Med*. 2014 Jul 30;6(247):247ra101.
283. Gao F, Cui Y, Jiang H, Sui D, Wang Y, Jiang Z, et al. Circulating tumor cell is a common property of brain glioma and promotes the monitoring system. *Oncotarget*. 2016 Nov 1;7(44):71330–40.
284. Shao H, Chung J, Balaj L, Charest A, Bigner DD, Carter BS, et al. Protein typing of circulating microvesicles allows real-time monitoring of glioblastoma therapy. *Nat Med*. 2012 Dec;18(12):1835–40.
285. Ricklefs FL, Alayo Q, Krenzlin H, Mahmoud AB, Speranza MC, Nakashima H, et al. Immune evasion mediated by PD-L1 on glioblastoma-derived extracellular vesicles. *Sci Adv*. 2018;4(3):eaar2766.
286. Hallal S, Ebrahimkhani S, Shivalingam B, Graeber MB, Kaufman KL, Buckland ME. The emerging clinical potential of circulating extracellular vesicles for non-invasive glioma diagnosis and disease monitoring. *Brain Tumor Pathol*. 2019 Apr;36(2):29–39.
287. Whitehead CA, Kaye AH, Drummond KJ, Widodo SS, Mantamadiotis T, Vella LJ, et al. Extracellular vesicles and their role in glioblastoma. *Crit Rev Clin Lab Sci*. 2019 Dec 22;1–26.
288. Yekula A, Minciacchi VR, Morello M, Shao H, Park Y, Zhang X, et al. Large and small extracellular vesicles released by glioma cells in vitro and in vivo. *J Extracell Vesicles*. 2020;9(1):1689784.
289. Naryzhny S, Volnitskiy A, Kopylov A, Zorina E, Kamyshinsky R, Bairamukov V, et al. Proteome of Glioblastoma-Derived Exosomes as a Source of Biomarkers. *Biomedicines*. 2020 Jul 16;8(7).
290. Hafeez U, Cher LM. Biomarkers and smart intracranial devices for the diagnosis, treatment, and monitoring of high-grade gliomas: a review of the literature and future prospects. *Neuro-Oncol Adv*. 2019 Dec;1(1):vdz013.
291. Hallal S, Ebrahim Khani S, Wei H, Lee MYT, Sim H-W, Sy J, et al. Deep Sequencing of Small RNAs from Neurosurgical Extracellular Vesicles Substantiates miR-486-3p as a Circulating Biomarker that Distinguishes Glioblastoma from Lower-Grade Astrocytoma Patients. *Int J Mol Sci*. 2020 Jul 13;21(14).
292. Koch CJ, Lustig RA, Yang X-Y, Jenkins WT, Wolf RL, Martinez-Lage M, et al. Microvesicles as a Biomarker for Tumor Progression versus Treatment Effect in Radiation/Temozolomide-Treated Glioblastoma Patients. *Transl Oncol*. 2014 Dec;7(6):752–8.
293. Osti D, Del Bene M, Rappa G, Santos M, Matafora V, Richichi C, et al. Clinical

Significance of Extracellular Vesicles in Plasma from Glioblastoma Patients. *Clin Cancer Res Off J Am Assoc Cancer Res.* 2019 Jan 1;25(1):266–76.

294. Zhao Z, Zhang C, Li M, Shen Y, Feng S, Liu J, et al. Applications of cerebrospinal fluid circulating tumor DNA in the diagnosis of gliomas. *Jpn J Clin Oncol.* 2020 Mar 9;50(3):325–32.

295. Cordova C, Syeda MM, Corless B, Wiggins JM, Patel A, Kurz SC, et al. Plasma cell-free circulating tumor DNA (ctDNA) detection in longitudinally followed glioblastoma patients using TERT promoter mutation-specific droplet digital PCR assays. *J Clin Oncol.* 2019 May 20;37(15_suppl):2026–2026.

296. Dong L, Li Y, Han C, Wang X, She L, Zhang H. miRNA microarray reveals specific expression in the peripheral blood of glioblastoma patients. *Int J Oncol.* 2014 Aug;45(2):746–56.

297. Li H-Y, Li Y-M, Li Y, Shi X-W, Chen H. Circulating microRNA-137 is a potential biomarker for human glioblastoma. *Eur Rev Med Pharmacol Sci.* 2016;20(17):3599–604.

298. Choppavarapu L, Kandi SM. Circulating microRNAs as Potential Biomarkers in Glioma: A Mini Review. *Endocr Metab Immune Disord Drug Targets.* 2020 Jul 30;

299. ParvizHamidi M, Haddad G, Ostadrahimi S, Ostadrahimi N, Sadeghi S, Fayaz S, et al. Circulating miR-26a and miR-21 as biomarkers for glioblastoma multiform. *Biotechnol Appl Biochem.* 2019 Mar;66(2):261–5.

300. Tabibkhoei A, Izadpanahi M, Arab A, Zare-Mirzaei A, Minaeian S, Rostami A, et al. Profiling of novel circulating microRNAs as a non-invasive biomarker in diagnosis and follow-up of high and low-grade gliomas. *Clin Neurol Neurosurg.* 2020;190:105652.

301. Huang S-W, Ali N, Zhong L, Shi J. MicroRNAs as biomarkers for human glioblastoma: progress and potential. *Acta Pharmacol Sin.* 2018 Sep;39(9):1405–13.

302. Mercatelli N, Galardi S, Ciafrè SA. MicroRNAs as Multifaceted Players in Glioblastoma Multiforme. *Int Rev Cell Mol Biol.* 2017;333:269–323.

303. Morokoff A, Jones J, Nguyen H, Ma C, Lasocki A, Gaillard F, et al. Serum microRNA is a biomarker for post-operative monitoring in glioma. *J Neurooncol.* 2020 Sep;149(3):391–400.

304. Yin J, Zeng A, Zhang Z, Shi Z, Yan W, You Y. Exosomal transfer of miR-1238 contributes to temozolomide-resistance in glioblastoma. *EBioMedicine.* 2019 Apr;42:238–51.

305. Swellam M, Ezz El Arab L, Al-Posttany AS, B Said S. Clinical impact of circulating oncogenic MiRNA-221 and MiRNA-222 in glioblastoma multiform. *J Neurooncol.* 2019 Sep;144(3):545–51.

306. Simonelli M, Dipasquale A, Orzan F, Lorenzi E, Persico P, Navarra P, et al. Cerebrospinal fluid tumor DNA for liquid biopsy in glioma patients' management: Close to the clinic? *Crit Rev Oncol Hematol.* 2020 Feb;146:102879.

Table 1: Description of advanced MRI techniques, metrics, and results of pseudoprogression (PsP) and true progression (TP).

Advanced MRI techniques		Metrics	Results for PsP/TP
Diffusion MRI			
DWI : Diffusion-Weighted MRI	Water diffusion within tissue (displacement of water molecules in brain parenchyma)	ADC: Apparent Diffusion Coefficient quantify the mobility of water molecules at the cellular level	ADC value: PsP>TP ADC ratio: PsP>TP
DTI : Diffusion Tensor Imaging	Direction of water diffusion	FA: Fractional Anisotropy measures the fraction of the diffusion that is anisotropic (diffusion asymmetry in a voxel)	FA value: TP>PsP FA ratio: TP>PsP
Perfusion MRI			
DSC: Dynamic Susceptibility Contrast MRI	T2/T2*-weighted technique measurement of vascular perfusion and permeability Exogenous gadolinium based contrast agent	rCBF: relative Cerebral Blood Flow measurement of the lesion blood flow compared to contralateral cerebral tissue (white or grey matter) rCBV: relative Cerebral Blood Volume measurement of the lesion blood volume compared to contralateral cerebral tissue (white or grey matter) PH: Peak Height reflects the total blood volume maximal signal intensity PSR: percentage of signal intensity recovery reflects capillary permeability	rCBF: TP>PsP rCBV: TP>PsP PH: TP>PsP PSR: PsP>TP
DCE: Dynamic Contrast Enhanced	T1-based technique measurement of	K^{trans}: Volume Transfer Constant between plasma and EES	K^{trans}: TP>PsP

MRI	vascular permeability Exogenous gadolinium based contrast agent	reflects gadolinium leakage rate from plasma to EES and microvascular permeability V_e: Volume of EES reflects cellularity and necrosis in EES and microvascular permeability V_p: Vascular plasma volume reflects blood plasma volume K_{ep}: Transfer constant from the EES into the plasma = K_{trans}/V_e	V_e: TP ≥ PsP V_p: TP ≥ PsP K_{ep}: TP = PsP
ASL: Arterial Spin Labeling	Brain tissue perfusion Magnetic arterial blood water protons as an endogenous tracer	CBF: Cerebral Blood Flow Blood volume through a cerebral region per unit of time	CBF: TP > PsP
Magnetic Resonance Spectroscopy			
MRS: Magnetic Resonance Spectroscopy	Reflects the distribution of chemical metabolites within a brain tissue volume	Cho: Choline Cr: Creatinine Lac: Lactate Lip: Lipid NAA: N-acetylaspartate	Cho/NAA: TP > PsP Cho/Cr: TP > PsP NAA/Cr: PsP > TP

Table 2: Review of the apparent diffusion coefficient (ADC) values in the literature for pseudoprogression (PsP) and true progression (TP).

Authors	N	Tumors	Parameters	Values		p value	Threshold	Se	Sp	PPV	NPV	Accuracy	
				PsP	TP								
Hein et al., 2004 (67)	18 (8)	HGG (GBM)	ADC ratio	1.82	1.43	<0.001	NA	NA	NA	NA	NA	NA	
			Mean ADC value	1.40	1.18	<0.006							
Asao et al., 2005 (64)	17 (5)	HGG (GBM)	Minimal ADC value	1.04	1.07	> 0.05	NA	NA	NA	NA	NA	NA	NA
			Mean ADC value	1.68	1.37	>0.05							
			Maximal ADC value	2.30	1.68	0.039							
Sundgren et al., 2006 (68)	28 (4)	Primary brain tumor (GBM)	Mean ADC value	1.12	1.27	0.01	NA	NA	NA	NA	NA	NA	NA
			ADC ratio	1.40	1.54	0.07							
Zeng et al., 2007 (74)	55 (19)	HGG (GBM)	Mean ADC value	1.39	1.20	<0.01	NA	NA	NA	NA	NA	NA	NA
			ADC ratio	1.69	1.42	<0.01							
Bobek-Billewics et al., 2010 (81)	8 (2)	Gliomas (GBM)	Mean ADC value	1.13	1.06	0.51	NA	NA	NA	NA	NA	NA	NA
			ADC ratio	1.55	1.55	0.98							
Xu et al., 2010 (66)	35 (17)	Gliomas (GBM)	Mean ADC value	1.54	1.23	0.0002	NA	NA	NA	NA	NA	NA	NA
			ADC ratio	1.62	1.34	0.0013							
Lee et al., 2012 (65)	20	HGG	Mean ADC value	1.349	1.040	<0.0001	1.200	80	83	NA	NA	NA	81
	22 (19)	HGG (GBM)	Mean ADC value	1.349	1.215	0.289							
Fink et al., 2012 (76)	38 (10)	Gliomas (GBM)	ADC ratio	1.43	1.14	0.035	≤1.28	72	80	91	50	74	
Agarwal et al., 2013 (47)	24	HGG	Mean ADC value	1.40	1.37	0.700	NA	NA	NA	NA	NA	NA	

Chu et al., 2013 (84)	30	GBM	Mean ADC value	1.329	1.269	0.616						
Alexiou et al., 2014 (78)	30 (27)	HGG (GBM)	ADC ratio	2.12	1.19	0.005	1.27	65	100	NA	NA	NA
Prager et al., 2015 (77)	68 (55)	HGG (GBM)	Median ADC lesion value	1.62	1.39	0.001						
			ADC ratio	1.585	1.482	0.288	≥1.6	95	63	NA	NA	NA
			Median ADC ROI value	1.2	1.1	0.128						
Bulik et al., 2015 (79)	24	GBM	Mean ADC value	1.373	1.160	<0.001	1.300	100	100	NA	NA	NA
Kazda et al., 2016 (80)	39	GBM	Mean ADC value	1.372	1.155	<0.001	1.313	98	100	NA	NA	NA
Reimer et al., 2017 (73)	35	GBM	Relative ADC			0.014	0.25	86	86	NA	NA	NA
Jena et al., 2017 (75)	35 (17)	Gliomas (GBM)	Mean ADC value	1.558	1.283	0.015	≤1.507	87	55	84	58	78

ADC: Apparent diffusion coefficient; **GBM:** Glioblastoma; **HGG:** High grade gliomas; **NA:** not available; **NPV:** Negative Predictive Value; **PPV:** Positive Predictive Value; **PsP:** Pseudoprogression; **ROI:** Region of interest; **TP:** True Progression; **Se:** Sensibility; **Sp:** Specificity

Table 3: Review of the perfusion MRI metrics in the literature and their statistical characteristics

Authors	N	Tumors	Parameters	Values		p	Threshold	Se	Sp	PPV	NPV	Accuracy
				PsP	TP							
Barajas <i>et al.</i>, 2009 (122)	57	GBM	Mean rCBV	1.57	2.38	<0.01	1.75	79	72			
			Max rCBV	4.63	8.16	<0.01						
			Min rCBV	0.95	1.61	<0.01						
			Mean rPH	1.25	2.7	<0.01	1.38	89	81			
			Max rPH	1.72	3.09	<0.01				NA	NA	NA
			Min rPH	0.82	1.31	<0.01						
			Mean rPSR	89.3	80.2	0.01	87.3	78	76			
			Max rPSR	92.5	100	0.05						
			Min rPSR	77.2	68.8	0.04						
Hu <i>et al.</i>, 2009 (95)	13 (9)	HGG (GBM)	Min rCBV	0.21	0.55		0.71	92	100			96
			Max rCBV	0.71	4.64					NA	NA	
Gasparetto <i>et al.</i>, 2009 (97)	12	GBM	Mean rCBV				1.8	100	87	80	100	92
Bobek-Billewics <i>et al.</i>, 2010 (81)	8 (2)	Gliomas (GBM)	Max rCBV	0.78	2.44	<0.001	≥1.7	NA	NA	NA	NA	NA
			Mean rCBV	0.49	1.46	<0.004	≥1.25					
Tsien <i>et al.</i>, 2010 (104)	27 (23)	HGG (GBM)	Mean rCBV	2.3	2.8	0.8	NA	NA	NA	NA	NA	NA
Kim <i>et al.</i>, 2010 (99)	10	HGG	Mean rCBV	2.53	5.72	0.01	3.69	100	100	NA	NA	NA

	(5)	(GBM)										
Heidemans-Hazelaar et al., 2010 (94)	32	GBM	Mean rCBV			<0.002	2.12	88	83	96	63	NA
Bisdas et al., 2011 (110)	18	HGG	Median K^{trans}	0.15	0.43	0.0051	>0.19	100	83			
			Median V_e	0.34	0.56	NS				NA	NA	NA
			Median K_{ep}	0.34	0.45	NS						
Gahramanov et al., 2011 (98)	14	GBM	Mean rCBV	0.7	2.7	NA	1.75	NA	NA	NA	NA	NA
Kong et al., 2011 (107)	59	GBM	Mean rCBV	1.49	2.85	0.003	>1.49	81	78	NA	NA	NA
Fink et al., 2012 (76)	38 (10)	Gliomas (GBM)	CBV ratio	1.31	3.62	<0.001	≥ 2.08	86	90	96	69	87
Hu et al., 2012 (96)	25	GBM	Mean rCBV				1.0	100	100	NA	NA	100
Young et al., 2013 (100)	20	GBM	Median rCBV	1.50	2.75	0.009	≤ 1.8	100	75			
			Mean rPH	1.34	3.04	<0.001	≤ 2.4	69	100			
			Mean PSR	1.01	0.84	<0.039	≤ 1.7	100	100	NA	NA	NA
Larsen et al., 2013 (28)	19 (13)	Gliomas (GBM)	Mean CBV	1.3	10.9	NA	2.0	100	100			
			Mean CBF	11.9	28.1	NA				NA	NA	NA
Seeger et al., 2013 (92)	40	HGG	Mean rCBF (DSC)	1.66	4.01	<0.01	2.24	77	85			80
			Mean rCBF (ASL)	1.66	2.41	0.063	2.18	54	85			69
			Mean rCBV	1.73	3.91	0.01	2.15	81	77	NA	NA	79
			Median K^{trans}	0.03	0.05	0.07	>0.058	62	80			69
			Maximum K^{trans}	0.047	0.08	0.046						

			V_e	0.15	0.27	0.10						
Alexiou <i>et al.</i>, 2014 (78)	30 (27)	HGG (GBM)	Mean rCBV	1.68	6.71	0.000	2.2	100	100	NA	NA	NA
D'Souza <i>et al.</i>, 2014 (93)	29 (13)	HGG (GBM)	Mean rCBV	3.01	0.8	NA	NA	NA	NA	NA	NA	NA
Shin <i>et al.</i>, 2014 (105)	31 (18)	Gliomas (GBM)	Mean rCBV	2.11	2.55	0.511	2.33	72	70	NA	NA	NA
			Mean rK^{trans}	1.69	2.52	0.399	2.1	61	80			
Yun <i>et al.</i>, 2015 (111)	33	GBM	Mean K^{trans}	0.23	0.44	0.004	0.347	59	94	91	68	76
			V_e	0.75	1.26	0.034	0.570	88	56	68	82	
			V_p	0.11	0.14	0.119						
Thomas <i>et al.</i>, 2015 (112)	37	GBM	Mean V_p	2.4	5.3	0.0002	>3.7	85	79	NA	NA	NA
			90 th percentile V_p	3.2	6.6	>0.0001	>3.9	85	92			
			Mean K^{trans}	3.5	7.4	0.002	>3.6	69	79			
			90 th percentile K^{trans}	4.2	9.1	0.0004						
Prager <i>et al.</i>, 2015 (77)	68 (55)	HGG (GBM)	Median rCBV _{lesion}	0.88	1.76	0.028	<1.07	75	100	NA	NA	NA
			Median rCBV _{roi}	1.625	2.575	0.032	<1.74	75	93			
			Median rPSR _{roi}	0.87	0.80	0.467						
Wang <i>et al.</i>, 2016 (85)	41	GBM	Max rCBV	2.90	4.75	0.007	4.06	62	80	NA	NA	NA
Jena <i>et al.</i>, 2017 (75)	35 (17)	Gliomas (GBM)	Mean rCBV	1.82	2.41	0.082	≥ 1.71	NA	NA	NA	NA	77
Boxerman <i>et al.</i>, 2017 (103)	9 (6)	HGG (GBM)	Mean rCBV	2.4	2.2	0.67	>2.4	67	40	NA	NA	NA

GBM: Glioblastoma; **HGG:** High Grade Glioma; **K_{ep}:** Transfer constant from the extracellular-extravascular space into the plasma; **K^{trans}:** Volume Transfer Constant; **NA:** not available; **NPV:** Negative Predictive Value; **PPV:** Positive Predictive Value; **PSP:** Pseudoprogession; **rCBF:** relative Cerebral Blood Flow; **rCBV:** relative Cerebral Blood Volume; **ROI:** Regio of Interest; **rPH:** relative Peak Height; **rPSR:** relative Percentage of Signal intensity Recovery; **TP:** True Progression; **Se:** Sensibility; **Sp:** Specificity; **V_e:** Volume of extravascular-extracellular space; **V_p:** Vascular plasma volume

Table 4: Review of the different publications regarding MRS and the reported threshold values, sensitivity (Se), specificity (Sp), positive predictive value (PPV), negative predictive value (NPV), and accuracy

Parameters	Authors	N	Tumors	Values		p	Threshold	Se	Sp	PPV	NPV	Accuracy
				PsP	TP							
Cho/NAA	Plotkin <i>et al.</i> , 2004 (131)	25 (10)	Gliomas (GBM)	0.74	1.51	<0.0001	1.17	89	83	NA	NA	88
	Weybright <i>et al.</i> , 2005 (129)	29	Primary brain tumors	1.31	3.48	<0.0001	1.8	NA	NA	NA	NA	NA
	Zeng <i>et al.</i> , 2007 (74)	55 (19)	HGG (GBM)	1.55	3.52	<0.01	NA	NA	NA	NA	NA	NA
	Smith <i>et al.</i> , 2009 (128)	33 (4)	Primary brain tumors (GBM)	1.43	3.20	0.0007	NA	85	69	81	NA	NA
	Bobek-Billewicz <i>et al.</i> , 2010 (81)	8 (2)	Gliomas (GBM)	2.11	1.9	0.51	NA	NA	NA	NA	NA	NA
	Elias <i>et al.</i> , 2011 (132)	25 (2)	Primary brain tumors (GBM)	1.39	2.81	0.0004	NA	NA	NA	NA	NA	NA
	Fink <i>et al.</i> , 2012 (76)	38 (10)	Gliomas (GBM)	0.84	2.87	0.002	NA	NA	NA	NA	NA	NA
	Seeger <i>et al.</i> , 2013 (92)	40	HGG	1.47	2.20	0.20	NA	NA	NA	NA	NA	NA
	Anbarloui <i>et al.</i> , 2015 (127)	33 (13)	Primary brain tumors (GBM)	1.46	2.72	<0.01	>1.8	84	75	NA	NA	81
Bulik <i>et al.</i> , 2015 (79)	24	GBM	0.77	2.00	<0.001	≥1.4	100	92	NA	NA	NA	

	Kazda <i>et al.</i> , 2016 (80)	39	GBM	0.74	2.13	<0.001	≥ 1.3	100	95	NA	NA	NA
Cho/Cr	Plotkin <i>et al.</i> , 2004 (131)	25 (10)	Gliomas (GBM)	0.95	1.38	0.030	1.11	89	83	NA	NA	88
	Weybright <i>et al.</i> , 2005 (129)	29	Primary brain tumors	1.57	2.52	<0.0001	1.8	NA	NA	NA	NA	NA
	Zeng <i>et al.</i> , 2007 (74)	55 (19)	HGG (GBM)	1.61	2.82	<0.01	2.5	78	86	NA	NA	NA
	Nakajima <i>et al.</i> , 2009 (130)	18 (8)	Gliomas (GBM)	2.25	3.17	NS	NA	NA	NA	NA	NA	NA
	Smith <i>et al.</i> , 2009 (128)	33 (4)	Primary brain tumors (GBM)	1.57	2.36	0.0001	NA	NA	NA	NA	NA	NA
	Bobek-Billewicz <i>et al.</i> , 2010 (81)	8 (2)	Gliomas (GBM)	1.84	2.23	0.2441	NA	NA	NA	NA	NA	NA
	Elias <i>et al.</i> , 2011 (132)	25 (2)	Primary brain tumors (GBM)	1.34	2.16	0.15	NA	NA	NA	NA	NA	NA
	Fink <i>et al.</i> , 2012 (76)	38 (10)	Gliomas (GBM)	1.57	2.57	0.021	NA	NA	NA	NA	NA	NA
	Seeger <i>et al.</i> , 2013 (92)	40	HGG	1.30	1.66	0.047	>1.12	85	50	NA	NA	72
	D'Souza <i>et al.</i> , 2014 (93)	29 (13)	HGG (GBM)	1.26	2.27	NA	≥ 0.7	83	42	NA	NA	NA
	Bulik <i>et al.</i> , 2015 (79)	24	GBM	0.82	0.86	0.317	≥ 1.405	NA	NA	NA	NA	91
	Jena <i>et al.</i> , 2017 (75)	35 (17)	Gliomas (GBM)	1.63	3.47	0.002	≥ 0.7	75	63	NA	NA	NA
Kazda <i>et al.</i> , 2016 (80)	39	GBM	0.64	0.89	0.013	NA	NA	NA	NA	NA	NA	

NAA/Cr	Plotkin <i>et al.</i> , 2004 (131)	25 (10)	Gliomas (GBM)	1.44	0.99	0.212	NA	NA	NA	NA	NA	NA
	Weybright <i>et al.</i> , 2005 (129)	29	Primary brain tumors	1.22	0.79	<0.0001	NA	NA	NA	NA	NA	NA
	Zeng <i>et al.</i> , 2007 (74)	55 (19)	HGG (GBM)	1.10	0.84	<0.01	NA	NA	NA	NA	NA	NA
	Smith <i>et al.</i> , 2009 (128)	33 (4)	Primary brain tumors (GBM)	1.14	0.85	0.0183	NA	NA	NA	NA	NA	NA
	Elias <i>et al.</i> , 2011 (132)	25 (2)	Primary brain tumors (GBM)	1.36	0.85	0.0033	NA	NA	NA	NA	NA	NA
	Seeger <i>et al.</i> , 2013 (92)	40	HGG	0.51	1.01	0.051	NA	NA	NA	NA	NA	NA
	Bulik <i>et al.</i> , 2015 (79)	24	GBM	0.99	0.45	<0.001	≤0.7	94	92	NA	NA	NA
	Kazda <i>et al.</i> , 2016 (80)	39	GBM	0.99	0.41	<0.001	≤0.7	97	95	NA	NA	NA
Cho/Lip	Anbarloui <i>et al.</i> , 2015 (127)	33 (13)	Primary brain tumors (GBM)	0.6	2.78	<0.01	>1.0	84	75	NA	NA	81
Lac/Cr	Zeng <i>et al.</i> , 2007 (74)	55 (19)	HGG (GBM)	0.45	1.28	0.01	NA	NA	NA	NA	NA	NA
Lip/Cr	Zeng <i>et al.</i> , 2007 (74)	55 (19)	HGG (GBM)	0.54	0.14	0.01	NA	NA	NA	NA	NA	NA
Lac/Cho	Nakajima <i>et al.</i> , 2009 (130)	18 (8)	Gliomas (GBM)	2.35	0.63	<0.01	1.05	89	100	NA	NA	NA
(Lac+Lip)/Cr	Bulik <i>et al.</i> , 2015 (79)	24	GBM	0.88	4.43	0.004	≥1.9	92	75	NA	NA	NA

	Kazda <i>et al.</i> , 2016 (80)	39	GBM	1.13	2.69	0.005	≥ 1.6	76	68	NA	NA	NA
Lac+Lip	Bulik <i>et al.</i> , 2015 (79)	24	GBM	3.50	10.77	0.004	≥ 4.8	100	67	NA	NA	NA
Cho	Bulik <i>et al.</i> , 2015 (79)	24	GBM	2.88	2.41	0.739	≤ 2.9	69	42	NA	NA	NA
NAA	Bulik <i>et al.</i> , 2015 (79)	24	GBM	2.88	1.19	<0.001	≤ 1.5	75	100	NA	NA	NA
Cr	Bulik <i>et al.</i> , 2015 (79)	24	GBM	2.74	2.49	0.243	≤ 2.6	56	67	NA	NA	NA

Cho:Choline; **Cr:**Creatinine; **Lac:**Lactates; **Lip:**Lipids; **NAA:**N-acetylaspartate; **NPV:** Negative Predictive Value; **PPV:** Positive Predictive Value; **PsP:** Pseudoprogression; **TP:** True Progression; **Se:** Sensibility; **Sp:** Specificity

Table 5: Different tracers and metrics of positron-emission tomography (PET).

PET tracers		Metrics	TP/PsP
FDG	2-deoxy-2-[fluorine-18]fluoro- D-glucose	SUV: standardized uptake value T/N: tumor uptake to normal hemispheric tissue uptake T/S: tumor uptake to striatum uptake L/N: lesion uptake to normal brain tissue uptake L/R: lesion uptake to contralateral cerebral white matter uptake TBR: tumor-to-brain ratio TNR: tumor-to-normal brain ratio SUV/BG: standardized uptake value/background TTP: time to peak	TP>PsP TP>PsP TP>PsP TP>PsP TP>PsP TP>PsP TP>PsP TP>PsP PsP>TP
FDOPA	¹⁸ F-fluoro-L-dopa		
FET	O-(2-[¹⁸ F]fluoroethyl)-L-tyrosine		
MET	¹¹ C-methyl-L-methionine		
FLT	3'-deoxy-3'[(18)F]-fluorothymidine		
Choline	¹¹ C-Choline		
FMISO	¹⁸ F-Fluoromisonidazole		
MLT	¹¹ C-Methyl-L-Tryptophan PET		
FCho	¹⁸ F-fluoromethylcholine		
FBPA	4-borono-2- ¹⁸ F-fluoro-phenylalanine		

PET: Positron Emission Tomography; **PsP:** Pseudoprogession; **TP:** True Progression

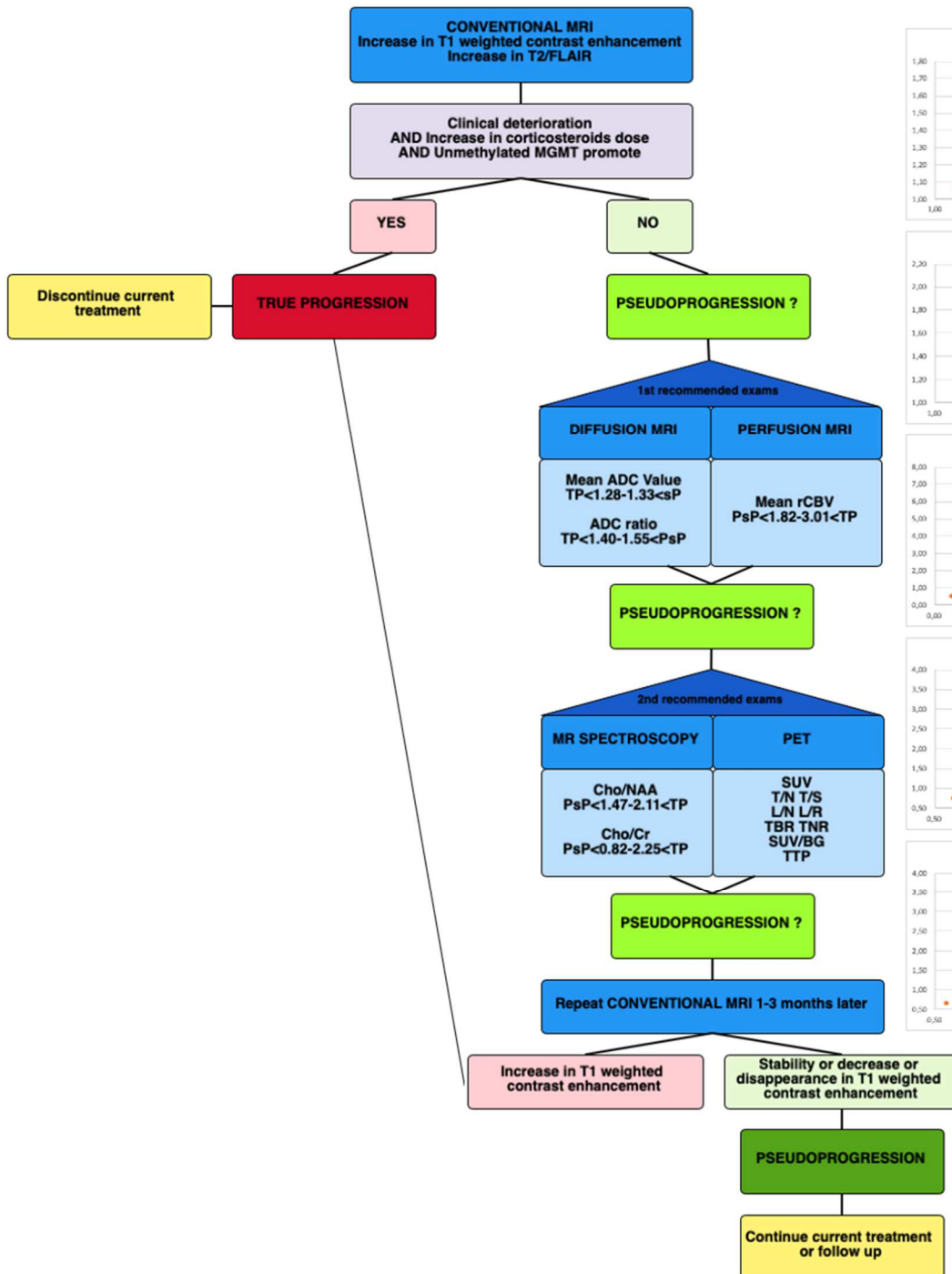
Table 6: Comparison of single imaging techniques to differentiate PsP versus TP according to the literature review.

Imaging technique		Features	Sensitivity	Specificity	Accuracy
Conventional MRI		High availability Low time acquisition Standardized protocol acquisition and recommendations (BPTI) More research and larger studies Limited sensitivity, specificity and accuracy Impact of treatment use (corticosteroids, antiangiogenics)	68-83%	25-77%	67%
Advanced MRI	Diffusion MRI	High availability Lack of standardized protocol Leakage correction needed Lower resolution Impact of treatment use (corticosteroids, antiangiogenics)	65-100%	55-100%	74-86%
	Perfusion MRI	Lower resolution Impact of treatment use (corticosteroids, antiangiogenics)	54-100%	40-100%	69-100%
MRS		High availability (monovoxel>multivoxel) Higher specificity and accuracy (monovoxel>multivoxel) Lower spatial resolution (monovoxel>multivoxel) Lack of reproducibly and variability (multivoxel>monovoxel) Long acquisition time (multivoxel>monovoxel) Long processing time (multivoxel>monovoxel) Long interpretation time (multivoxel>monovoxel) Lack of standardized threshold and various metabolic ratios (multivoxel>monovoxel) Signal contamination (lipids, water) (multivoxel>monovoxel) Impact of treatment use (corticosteroids, antiangiogenics), measurable	75-100%	40-95%	72-93%
PET	FDG	Standardized protocols and guidelines Higher sensitivity and accuracy	46-86%	22-100%	57-63%
	FDOPA	Variable availability Variable cerebral activity	84-100%	43-100%	78-96%

	FET	Variable half-life Variable stability Poor resolution	68-100%	70-100%	71-96%
	MET		75-100%	60-100%	75-94%
	FLT		91-100%	0-100%	Need additional researches
	FMISO		Need additional researches	Need additional researches	Need additional researches

BPTI: International Brain Tumor Imaging; **FDG:** Fluoro-Deoxy-Glucose; **FDOPA:** Fluoro-L-Dopa; **FET:** Fluoroethyl-L-Tyrosine; **FLT:** F-Fluorothymidine; **FMISO:** F-fluoromisonidazole; **MET:** methyl-L-methionine; **MRI:** Magnetic Resonance Imaging; **MRS:** Magnetic Resonance Spectroscopy; **PET:** Positron Emission Tomography

Figure 1: Clinical decisional diagram between pseudoprogression (PsP) and true progression (TP)



From the table 2 to the table 4

